



HAL
open science

Comprehensive study on the reactivity and mechanical properties of alkali-activated metakaolin at high H₂O/Na₂O ratios

Faten Souayfan, Emmanuel Rozière, Christophe Justino, Michaël Paris, Dimitri Deneele, Ahmed Loukili

► To cite this version:

Faten Souayfan, Emmanuel Rozière, Christophe Justino, Michaël Paris, Dimitri Deneele, et al.. Comprehensive study on the reactivity and mechanical properties of alkali-activated metakaolin at high H₂O/Na₂O ratios. *Applied Clay Science*, 2023, 231, pp.106758. 10.1016/j.clay.2022.106758 . hal-03910448

HAL Id: hal-03910448

<https://hal.science/hal-03910448v1>

Submitted on 6 Mar 2023

HAL is a multi-disciplinary open access archive for the deposit and dissemination of scientific research documents, whether they are published or not. The documents may come from teaching and research institutions in France or abroad, or from public or private research centers.

L'archive ouverte pluridisciplinaire **HAL**, est destinée au dépôt et à la diffusion de documents scientifiques de niveau recherche, publiés ou non, émanant des établissements d'enseignement et de recherche français ou étrangers, des laboratoires publics ou privés.

Applied Clay Science

A comprehensive study on the reactivity and the mechanical properties of alkali-activated metakaolin at high H₂O/Na₂O ratios

--Manuscript Draft--

Manuscript Number:	CLAY18449R2
Article Type:	Research Paper
Keywords:	Geopolymer; Metakaolin; water content; Reaction degree; mechanical properties; Viscoelastic properties
Corresponding Author:	Emmanuel Roziere, Ph.D. Ecole centrale de Nantes Nantes, Pays de la Loire FRANCE
First Author:	Faten Souayfan
Order of Authors:	Faten Souayfan Emmanuel Roziere, Ph.D. Christophe Justino Michaël Paris Dimitri Deneele Ahmed Loukili
Abstract:	<p>This study focused on the influence of high H₂O/Na₂O ratios (higher than 20) on the properties of metakaolin-based geopolymers in fresh and hardened states while keeping constant Si/Al and Na/Al atomic ratios. The increase in H₂O/Na₂O ratio from 21 to 34 resulted in a decrease of 7-day compressive strength from 10 to 0.025 MPa. This can be attributed to the influence of water on the reactivity of the precursor, which was demonstrated by nuclear magnetic resonance (NMR) spectroscopy and porosity evolution as the water is not chemically bound. Increasing H₂O/Na₂O ratio did not change the geopolymer structure of reaction products. A correlation was observed between the reaction degree deduced from NMR spectral decomposition and the cumulated released heat obtained using isothermal calorimetry. The maximum loss tangent, obtained using dynamic rheology, was linearly related to strength development.</p>
Suggested Reviewers:	<p>Hamza Güllü Gaziantep University of Science and Technology hgullu@gantep.edu.tr He has worked on the rheology on geopolymers for grouting and deep soil mixing</p> <p>Marcello Romagnoli University of Modena and Reggio Emilia romagnoli.marcello@unimore.it He has co-authored papers on the rheological behaviour of alkali-activated materials</p> <p>Kedsarin Pimraksa Chiang Mai University Faculty of Science kedsarin.p@cmu.ac.th He has studied the influence of chemical ratios on the properties of geopolymers</p> <p>Marina Clausi University of Pavia marina.clausi01@universitadipavia.it She has studied metakaolin-based geopolymers</p>
Response to Reviewers:	<p>Reviewer #1 Author made all deserved revision, now the paper could be accepted for the publication.</p> <p>Reviewer #2 The authors have addressed most of my Comments and the manuscript could be acceptable now.</p>

Reviewer #3

The authors have addressed the manuscript carefully. However, there are still some problems.

1. In Question 6, I think the authors should define "high" H₂O/Na. In what level is high? Higher than 20?

A precision has been added in abstract and introduction.

It was reported that an H₂O/Na₂O ratio between 10 and 20 is necessary to reach significant strength for a structural geopolymer (Cui, 2019).

High molar H₂O/Na₂O ratios (higher than 20) can be expected to result in a tradeoff between workability, mechanical properties, and durability.

2. Abstract is so general. Abstract must be enriched via valuable results which pave the way for understanding the audiences.

The abstract has been rewritten in the new version of the manuscript by reporting quantitative data and results. 80 % of the abstract reported the main results of this work. Authors will be thankful and open to any suggestions to modify and improve the abstract.

3. Wrong citation format: Cui et al. (Cui, 2019); (Pouhet et al., 2019) observed a; uengsuwattananon et al. (Juengsuwattananon et al., 2019) correlated

The citation format has been corrected in the text.

4. The following references can be cited as recent research advance related to the present study:

<https://doi.org/10.1016/j.clay.2019.105375>

<https://doi.org/10.1016/j.clay.2022.106412>

<https://doi.org/10.1016/j.conbuildmat.2020.121186>

<https://doi.org/10.1016/j.clay.2020.105769>

<https://doi.org/10.1016/j.cemconcomp.2022.104768>

Authors thank the reviewer for the references which have been incorporated in the text.

5. The conclusion should be more concise.

Compared to the previous version of the manuscript, the conclusion part has been revised to highlight the main findings.

Manuscript Number: CLAY18449R1

Title: A comprehensive study on the reactivity and the mechanical properties of alkali-activated metakaolin at high H₂O/Na₂O ratios

Faten Souayfan, Emmanuel Roziere, Christophe Justino,

Michaël Paris, Dimitri Deneele, Ahmed Loukili

Authors answers:

The authors would like to thank the reviewers for their efforts in handling this scientific work. The interesting remarks are gratefully acknowledged and will definitely improve the quality of this paper. All comments and suggestions have been addressed in the new version of the manuscript. The modifications are marked in **blue** characters in the revised manuscript to facilitate the review process. The table below presents the changes performed and responses to the reviewers' comments and recommendations, in the order they were raised.

Reviewer #1

Author made all deserved revision, now the paper could be accepted for the publication.

Reviewer #2

The authors have addressed most of my Comments and the manuscript could be acceptable now.

Reviewer #3

The authors have addressed the manuscript carefully. However, there are still some problems.

1. In Question 6, I think the authors should define "high" H₂O/Na. In what level is high? Higher than 20?

A precision has been added in abstract and introduction.

It was reported that an H₂O/Na₂O ratio between 10 and 20 is necessary to reach significant strength for a structural geopolymer (Cui, 2019).

High molar H₂O/Na₂O ratios (higher than 20) can be expected to result in a tradeoff between workability, mechanical properties, and durability.

2. Abstract is so general. Abstract must be enriched via valuable results which pave the way for understanding the audiences.

The abstract has been rewritten in the new version of the manuscript by reporting quantitative data and results. 80 % of the abstract reported the main results of this work. Authors will be thankful and open to any suggestions to modify and improve the abstract.

3. Wrong citation format: Cui et al. (Cui, 2019); (Pouhet et al., 2019) observed a; uengsuwattananon et al. (Juengsuwattananon et al., 2019) correlated

1
2
3
4
5
6
7
8
9
10
11
12
13
14
15
16
17
18
19
20
21
22
23
24
25
26
27
28
29
30
31
32
33
34
35
36
37
38
39
40
41
42
43
44
45
46
47
48
49
50
51
52
53
54
55
56
57
58
59
60
61
62
63
64
65

The citation format has been corrected in the text.

4. The following references can be cited as recent research advance related to the present study:

<https://doi.org/10.1016/j.clay.2019.105375>

<https://doi.org/10.1016/j.clay.2022.106412>

<https://doi.org/10.1016/j.conbuildmat.2020.121186>

<https://doi.org/10.1016/j.clay.2020.105769>

<https://doi.org/10.1016/j.cemconcomp.2022.104768>

Authors thank the reviewer for the references which have been incorporated in the text.

5. The conclusion should be more concise.

Compared to the previous version of the manuscript, the conclusion part has been revised to highlight the main findings.

Please, find attached a revised version of our manuscript. We hope these answers will meet your expectations and that the processing of this paper will resume normally.

Sincerely

[Click here to view linked References](#)

1 **Comprehensive study on the reactivity and mechanical properties of alkali-** 2 **activated metakaolin at high H₂O/Na₂O ratios**

3 Faten Souayfan^a, Emmanuel Roziere^a, Christophe Justino^b, Michaël Paris^c, Dimitri Deneele^{c,d},
4 Ahmed Loukili^a

5 ^a Civil engineering and Mechanics Research Institute (GeM), UMR-CNRS 6183, Ecole Centrale
6 de Nantes, 1 rue de la Noe – 44321 Nantes, France

7 ^b Soletanche-Bachy, Chemin des Processions – 77130 Montereau Fault Yonne, France

8 ^c Université de Nantes, CNRS, Institut des Matériaux Jean Rouxel, IMN, F-44000 Nantes,
9 France

10 ^d GERS-LGIE, Université Gustave Eiffel, IFSTTAR, F-44344 Bouguenais, France

11 **Abstract**

12 This study focused on the influence of high H₂O/Na₂O ratios ([higher than 20](#)) on the properties
13 of metakaolin-based geopolymers in fresh and hardened states while keeping constant [Si/Al](#)
14 [and Na/Al atomic ratios](#). [The increase in H₂O/Na₂O ratio from 21 to 34 resulted in a decrease](#)
15 [of 7-day compressive strength from 10 to 0.025 MPa](#). This can be attributed to the influence of
16 water on the reactivity of the precursor, which was demonstrated [by nuclear magnetic resonance](#)
17 [\(NMR\) spectroscopy](#) and porosity evolution as the water is not chemically bound. [Increasing](#)
18 [H₂O/Na₂O ratio did not change the geopolymer structure of reaction products](#). A correlation
19 was observed between the reaction degree deduced from NMR spectral decomposition and the
20 cumulated released heat obtained using isothermal calorimetry. The maximum loss tangent,
21 obtained using dynamic rheology, ~~appeared to be a useful indicator for quantifying the influence~~
22 ~~of water from the early stage, as it~~ was linearly related to strength development.

23 **Keywords:** Geopolymer, Metakaolin, Water content, Reaction degree, Mechanical properties,
24 Viscoelastic properties

25 **1. Introduction**

26 Geopolymer materials can be obtained by activating solid aluminosilicate sources under the
27 action of an alkaline solution at a high pH (Provis, 2014). Under these conditions, a precursor
28 is dissolved to enrich the medium with reactive monomers, followed by the orientation,
29 polycondensation, and formation of a three-dimensional rigid network (Provis, 2013). Calcined
30 clay containing metakaolin is a common aluminosilicate precursor used for geopolymer
31 formation (Liu et al., 2020; Yang et al., 2022; Zhang et al., 2021, 2020) . Among the different
32 options, kaolinitic clays are widely considered because of their availability (Scrivener et al.,
33 2018) and environmental impact (Turner and Collins, 2013). The alkaline activation of these
34 calcined clays results in the formation of a geopolymer structure (Cherki El Idrissi et al., 2018a;
35 Costa et al., 2021) (Garcia-Lodeiro et al., 2015) instead of hydration products with chemically
36 bound water. Therefore, geopolymers are considered a method to improve the technical
37 performance and sustainability of construction materials in different applications (Clausi et al.,
38 2016; Güllü et al., 2020; Hassan et al., 2019; Wu et al., 2019). Metakaolin-based geopolymers
39 are now being considered for civil engineering applications, including soil improvement and
40 the containment of polluted soils. These studies require the use of grouts, i.e. relatively diluted
41 mixtures, incorporated in existing soil. Here, a high strength is not the main requirement, but
42 low water permeability and high durability in potentially aggressive waters are expected
43 (Yaghoubi et al., 2019; Zhang et al., 2015).

44 Metakaolin-based geopolymers are expected to satisfy several specifications in fresh and
45 hardened states, depending on the intended application. For example, grouts used for soil
46 improvement with a high water-to-solid ratio should be stable during storage before use and
47 have relatively low viscosities, and these properties should be maintained during the entire
48 duration of the process (Aboulayt et al., 2020, 2018; Güllü et al., 2019). In structural
49 applications, mortar and concrete should be designed with workability and strength equivalent

50 to cement-based materials (Hassan et al., 2019). Therefore, independent of the application and
51 durability requirements, the rheology of a material in its fresh state is vital. Aboulayt et al.
52 (Aboulayt et al., 2018) demonstrated the ability of metakaolin grouts to satisfy different
53 specifications, including open time; however, they have a relatively high viscosity. The
54 relatively high specific surface area of metakaolin and the properties of sodium silicate
55 solutions (Gadkar and Subramaniam, 2019; Hwalla et al., 2020; San Nicolas et al., 2013) result
56 in high viscosity and poor workability, which limits its potential uses. The viscosity of
57 metakaolin geopolymers at low shear rates has been observed to depend on their solid content
58 (Leonelli and Romagnoli, 2015). (Favier et al., 2013) reported that the high viscosity of an
59 activated metakaolin binder is primarily controlled by the viscosity of the alkaline silicate
60 solution and not by the solid fraction, which explains why the common plasticizers used in the
61 concrete industry are not efficient in metakaolin-based geopolymers. Consequently, the mixture
62 proportions and associated ratios are key parameters for controlling the properties of
63 metakaolin-based geopolymers. Water content is a major parameter for controlling the
64 properties in the fresh state.

65 Additionally, in specific applications, such as deep soil mixing (Bruno et al., 2018), water is
66 considered a crucial parameter that affects the properties of hardened materials, even if high
67 strength is not required. When the grout is mixed with the soil, water from the soil is added to
68 the initial mixture; thus, the total water-to-solid ratio increases significantly. Thus, the influence
69 of high water content must be quantified to determine its influence in both fresh and hardened
70 states in highly diluted systems.

71 Water influences geopolymerization reactions as it is involved in dissolution, hydrolysis, and
72 polycondensation reactions (Weng and Sagoe-Crentsil, 2007). (Sathonsaowaphak et al., 2009)
73 reported that water is the only efficient lever for the workability of geopolymers. (Cherki El
74 Idrissi et al., 2018b) demonstrated that a high water content is required to achieve the expected

75 rheological properties of a metakaolin grout, but it may affect its mechanical properties. Other
 76 authors (Paniyas et al., 2007; Provis et al., 2009; Souayfan et al., 2022; Yahya et al., 2015) proved
 77 that water content is a crucial parameter in the synthesis of geopolymers for the development
 78 of mechanical strength.

79 **Table 1** lists the experimental conditions used in recent studies on the influence of water
 80 content. [Cui \(2019\)](#) demonstrated that a higher H_2O/Na_2O ratio in the range of 13–17
 81 contributes to the dissolution of the active component of the precursor but hinders the
 82 polymerization reaction of monomeric and oligomeric gels. [Juengsuwattananon et al. \(2019\)](#)
 83 correlated the phase structures of reaction products with different initial chemical compositions,
 84 including different H_2O/Na_2O ratios (from 10 to 20). Depending on the initial composition,
 85 zeolitic or geopolymer structures are formed, which directly affect strength development.
 86 [Pouhet et al. \(2019\)](#) observed a linear decrease in the mechanical strength of a geopolymer and
 87 reported that the major part of the initial water was not bonded to the structure. Thus, water not
 88 only influences the rheological properties but also the advancement of the reaction, structure,
 89 and strength of geopolymers. Therefore, a comprehensive study is necessary to understand the
 90 features of nanostructures (Etemadi et al., 2021; Mahdavi et al., 2022; Zinatloo-Ajabshir et al.,
 91 2022, 2021) to explain the properties at the macroscopic scale.

92 **Table 1. Comparison of this study with previous recent works on the influence of water**
 93 **content under different experimental conditions**

	(Juengsuwattananon et al., 2019)	(Pouhet et al., 2019)	(Cui, 2019)	Present study
H_2O/Na_2O	From 10 to 20	-	From 13 to 17	From 21 to 34
Na/Al-Si/Al	Variables	Variables	Constant	Constant
Water/solid ratio	From 0.51 to 1.5	From 0.35 to 0.75	-	From 0.65 to 1
Precursor	Metakaolin	Metakaolin	Fly ash class F	Metakaolin

State	Hardened material	Hardened material	Fresh and hardened material	Fresh and hardened material
Techniques	CS/SEM/XRD	CS/MIP/SEM/XRD/TGA	IC/XRD/FTIR/MIP/SEM/TGA/CS	IC/RMN/Dynamic rheology/Water porosity/CS

94 *CS: compressive strength; XRD: X-ray diffraction; SEM: scanning electron microscopy;
95 TGA: thermogravimetric analysis; MIP: mercury intrusion porosimetry; IC: isothermal
96 calorimetry; FTIR: Fourier-transform infrared spectroscopy

97 Few studies investigated the influence of water content independent of other parameters. Most
98 existing studies focused on the liquid-activator-to-solid-precursor and SiO₂-to-Na₂O ratios.
99 Their variations influence the H₂O/Na₂O ratio and other molar ratios. Therefore, predicting the
100 influence of water content on the behavior and engineering properties of metakaolin-based
101 geopolymers from fresh to hardened states is still difficult. It was reported that an H₂O/Na₂O
102 ratio between 10 and 20 is necessary to reach significant strength for a structural geopolymer
103 (Cui, 2019). High molar H₂O/Na₂O ratios (higher than 20) can be expected to result in a tradeoff
104 between workability, mechanical properties, and durability, only a few investigations addressed
105 such high molar ratios, as shown in Table 1. Hence, a comprehensive study on the influence of
106 higher H₂O/Na₂O ratios on short- and long-term properties, with controlled molar ratios, is
107 required.

108 Therefore, the main aim of this paper is to highlight the effects of the H₂O/Na₂O ratio on the
109 reactivity and mechanical properties of metakaolin-based geopolymers to provide useful
110 information for the design of materials with different specifications. Several sodium silicate-
111 activated metakaolin mixtures were designed by varying H₂O/Na₂O while maintaining constant
112 Si/Al and Na/Al atomic ratios. The effect of H₂O/Na₂O is of primary importance in the design
113 of metakaolin-based geopolymers. This article provides a comprehensive study on the effect of
114 H₂O/Na₂O and a base of knowledge on different techniques and combined approaches to
115 provide useful methodologies for further research. The behaviors of fresh and hardened

116 materials were investigated through isothermal calorimetry and dynamic rheology in the linear
117 viscoelastic range. Dynamic rheology provides deep insight into the evolution of the early
118 development of mechanical properties (Rifaai et al., 2019). The local structures of the hardened
119 grouts were investigated using nuclear magnetic resonance (NMR). The compressive strength
120 was determined at different ages and correlated to the maximum loss tangent ($\tan \delta$) obtained
121 using rheological tests and the degree of reaction calculated from NMR spectra decomposition.
122 The actual porosity was also assessed to understand the influence of the $\text{H}_2\text{O}/\text{Na}_2\text{O}$ ratio on
123 strength.

124

125 2. Experimental program

126 2.1. Materials and mixtures preparation

127 The studied mixtures were designed using metakaolin as a precursor and an activation solution
128 based on sodium silicate. Metakaolin was produced using the flash calcination of clay from
129 Fumel, France. The relatively high silica content of metakaolin (67.1 wt.%) was due to a
130 significant proportion of quartz. The proportion of the pure metakaolin $\text{Al}_2\text{O}_3(\text{SiO}_2)_2$ phase was
131 43 wt.%. The mass fractions of CaO, Fe_2O_3 , MgO, TiO_2 , and Na_2O were 1.1%, 2.6%, 0.11%,
132 1.3%, and 0.01%, respectively. The average particle size of metakaolin was 18 μm , its density
133 was 2.63, and its specific surface area was 16.5 m^2/g as determined using N_2 sorption and the
134 Brunauer–Emmett–Teller (BET) method.

135 The activation solution was prepared by diluting a sodium silicate solution with a fixed
136 $\text{SiO}_2/\text{Na}_2\text{O}$ ratio of 1.7 and a dry content of 44% in demineralized water. The sodium silicate
137 solution was specially designed with a relatively high Na_2O content to reduce the subsequent
138 addition of NaOH as much as possible during the preparation of the studied mixtures. A very
139 low NaOH content was added in pellets to adjust the Na/Al ratio to 1. The molar ratio of SiO_2
140 to Na_2O in the activator and the chemical composition was selected as recommended in the
141 literature to facilitate good dissolution of the precursor (Duxson et al., 2007).

142 Four mixtures were designed with constant Si/Al and Na/Al molar ratios and different
143 $\text{H}_2\text{O}/\text{Na}_2\text{O}$ ratios (Table 2). The precursor to sodium silicate solution mass ratio was kept
144 constant for all compositions. The water-to-solid ratio was calculated using the total water in
145 the mixture, including the added demineralized water, water fraction in the activation solution,
146 and total amount of solid, including the precursor and solid fraction of the activation solution.
147 The total NaOH content of the activating solution included NaOH from the sodium silicate
148 solution and added NaOH pellets. The total NaOH concentration decreased with the water-to-

149 solid ratio but remained relatively high. Based on a previous study (Cherki El Idrissi, 2019),
 150 bentonite and dispersant were added to stabilize and deflocculate the material, respectively. The
 151 activation solution was prepared first, and then the powders were added and stirred in a high-
 152 shear mixer for 5 min to ensure proper homogenization. The specimens were sealed and stored
 153 at 20 °C before characterization in a hardened state.

154

155 **Table 2 Compositions of the studied mixtures**

Mixtures		MK21	MK24	MK28	MK34
Materials	Density	Compositions (g/l)			
Metakaolin	2.63	732	671	604	518
Na-silicate	1.55	636	583	525	450
NaOH	1.46	3.3	3.0	2.7	2.3
Bentonite	2.5	9	11	13	15
Dispersant	1.4	5.5	5	4.5	4
water	1	310	367	429	511
Water to solid ratio (W/S wt.%)		0.65	0.75	0.85	1.04
Volume fractions (%)	Water	66	68	72	76
	Solid phases	34	32	28	24
Atomic ratios	Si/Al	1.83	1.83	1.83	1.83
	Na/Al	1	1	1	1
Molar ratio	H ₂ O/Na ₂ O	21	24	28	34
Total NaOH in activating solution (mol/l solution)		5.29	4.71	4.00	3.25

156

157 2.2. Testing procedures

158 2.2.1. Nuclear magnetic resonance (NMR)

159 Solid-state ^{29}Si NMR spectroscopy was performed using a Bruker Avance III 300 MHz (7 T)
160 spectrometer and a 7 mm magic angle spinning (MAS) probe, whereas ^{27}Al MAS NMR
161 spectroscopy was performed using a 500 MHz Bruker Avance III with a 2.5 mm MAS probe.
162 For ^{27}Al acquisition, the MAS speed was 30 kHz and the repetition time was set to 1 s. ^{27}Al
163 spectra were determined using a single $\pi/13$ excitation pulse for a radiofrequency field of 12
164 kHz. Chemical shifts were referenced against an $\text{Al}(\text{NO}_3)_3$ solution. For ^{29}Si acquisition, the
165 MAS speed was 5 kHz and the repetition time was set to 5 s. ^{29}Si MAS NMR spectra were
166 acquired with a single $\pi/2$ excitation of 5.5 μs . The recycle delay between scans was set to 5 s.
167 Chemical shifts were referenced against tetramethylsilane (TMS). The analysis was performed
168 on fragments obtained from crushed samples sawn from the core of hardened specimens after
169 7-, 28-, and 90-day curing in a moist room at 95% relative humidity (RH). The fragments used
170 for these tests were ground to pass through an 83 μm sieve.

171 The software Dmfit (Massiot et al., 2002) was used to decompose the ^{29}Si spectra to calculate
172 the degree of reaction. The ^{29}Si spectra were decomposed into a formed phase and a signal
173 representing remnant metakaolin. Remnant metakaolin was considered by fitting a scaled
174 component spectrum calculated from the ^{29}Si spectrum of raw metakaolin. The Gaussian lines
175 used for the decomposition of ^{29}Si spectra were defined by their intensity, peak position, and
176 full width at half height (FWHH). The overall degree of reaction RD_{ov} (**Equation 1**) could be
177 determined from the amount of formed phase in terms of Si mol%. Therefore, the reaction
178 degree was equivalent to the amount of product. In addition, the reaction degree of metakaolin
179 RD_{mk} was calculated using **Equation 2**, where $X(\text{Si})_{mk}$ and R_{mk} refer to the silicon originating
180 from metakaolin of known chemical composition and the remnant metakaolin, respectively

181 (Table 2). Only the amorphous fraction of the metakaolin was considered in the calculation.
182 The contribution of quartz at -107 ppm was not considered because of the very long relaxation
183 delays associated with the Q⁴ sites in quartz, which means that they could not be captured
184 quantitatively in the spectra. Additionally, quartz was assumed to remain unreactive during the
185 process; thus, it was not considered in the reaction progress.

$$RD_{ov}(Si) = \frac{\text{Moles of Si in product phase}}{\text{Moles of total Si in sample}} \quad \text{Equation 1}$$

$$RD_{mk} = \frac{X(Si)_{mk} - R_{mk}}{X(Si)_{mk}} \quad \text{Equation 2}$$

186 2.2.1. Isothermal Calorimetry

187 The short-term reactivities of the studied mixtures were characterized using an isothermal
188 calorimeter (TAM Air). The temperature was maintained at 20 °C throughout the tests. The
189 heat flow was measured, and the cumulative heat was deduced by integrating the measured
190 flux. The measurements were conducted for seven days after the end of mixing. The
191 advancement of the geopolymerization reaction was approximated by the extent of the reaction,
192 defined as the ratio of the cumulative heat at time t (Q (t)) to the ultimate heat (Q_∞). The ultimate
193 heat Q_∞ was determined by plotting the cumulative heat as a function of 1/√t (Lenormand et
194 al., 2015). A linear evolution was observed for small 1/√t values. Q_∞ was estimated as the
195 intersection of this linear function with the y-axis.

196 2.2.2. Dynamic rheology

197 Dynamic rheological measurements were performed using a Discovery Hybrid Rheometer from
198 TA Instruments with a vane-type configuration at a constant temperature of 20 °C. Vane
199 geometry was used to minimize the disturbance of the material during the introduction of the

200 geometry and to avoid wall slip (Saak et al., 2001). The diameters of the cup and bob were 30.36
201 and 26.198 mm respectively, providing a shear gap of 4 mm.

202 The properties of the studied mixtures in their fresh state were monitored using dynamic
203 rheology in the linear viscoelastic domain. First, the linear viscoelastic domain was determined
204 such that the measurements were nondestructive. Fresh materials were prepared and
205 immediately introduced into the bowl of the rheometer. When the material was transferred to
206 the measurement cell, residual stresses were generated and relaxed. Hence, before each test, a
207 pre-shear at 200 s^{-1} for 60 s was applied, followed by oscillation with a strain of 5% at a
208 pulsation rate of 5 rad/s (Rifaai et al., 2019) (Poulesquen et al., 2011). After the preconditioning
209 step, all experiments were performed with a strain of 0.05% (in the linear region) and pulsation
210 rate of 10 rad/s. The elastic modulus (G'), viscous modulus (G''), and loss tangent ($\tan \delta =$
211 G''/G') were analyzed during the first few hours.

212 **2.2.3. Water porosity**

213 The porosity of the material was measured at 28 and 90 days on cylindrical specimens. The
214 specimens were first saturated with water under a vacuum according to the French standard
215 procedure NF P18-459 (2010) (NF P18-459, 2010) for 4 h in air and 44 h in water. The samples
216 were then placed in an oven at $105 \text{ }^\circ\text{C}$ and weighed every day until the mass variation was lower
217 than 0.05% within 24 h to determine the dry mass. Porosity was deduced from the saturated
218 surface dry mass (SSD), dry mass (D) in air, and mass (W) in water (Equation 3).

$$\varepsilon (\%) = \frac{SSD - D}{SSD - W} * 100 \quad \text{Equation 3}$$

219 **2.2.4. Compressive strength**

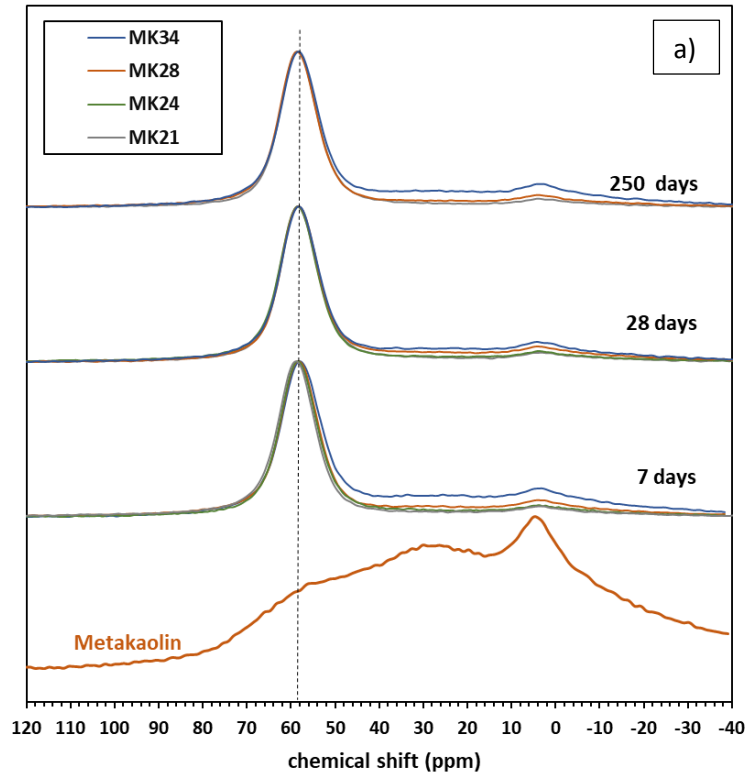
220 The test was conducted on a 100 kN press. The load rate was 1.9 kN/s until failure (NF EN
221 12390-3, 2019). Compression tests were performed on cylinders 70 mm in diameter and 140
222 mm in height at the ages of 7, 28, and 90 days. The height/diameter ratio of the tested cylinders
223 was 2, as recommended by the NF EN 12390-1 standard (NF EN 12390-1, 2012). The samples
224 were molded and cured in a room at 95% RH until compressive testing.

225 **3. Results and discussion**

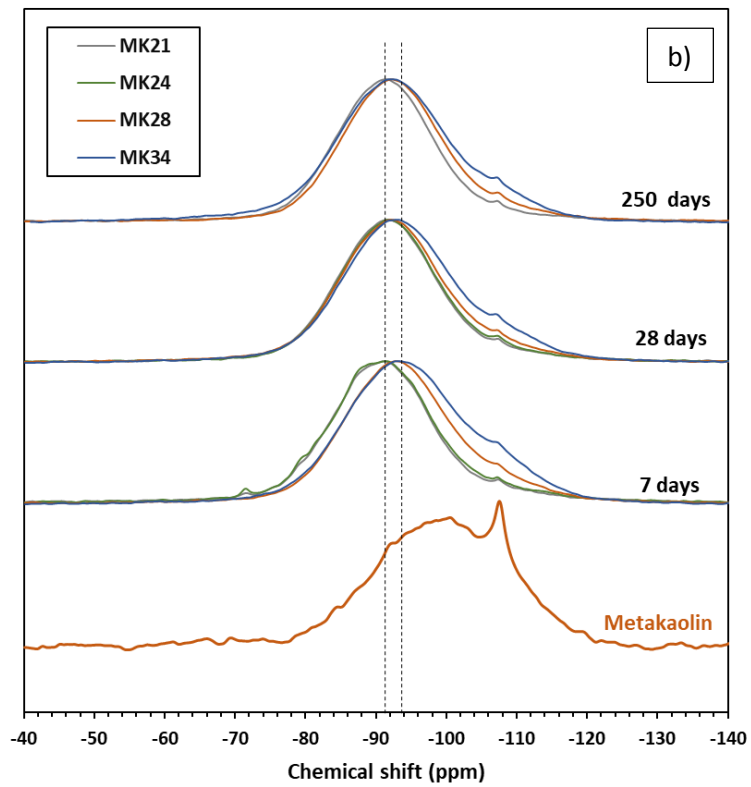
226 **3.1. Chemical characterization**

227 **3.1.1. Influence of H₂O/Na₂O on local structure**

228 ²⁷Al NMR spectra of the raw and activated metakaolin cured for 7, 28, and 250 days are
229 presented in Figure 1.a. Raw metakaolin exhibited three overlapping peaks with maxima at 55,
230 28, and 4 ppm attributed to four-, five-, and six-coordinated aluminum, respectively. The
231 activated metakaolin systems contained one predominant signal centered at 58 ppm
232 corresponding to tetrahedrally coordinated aluminum AlO₄(4Si) in the reaction products,
233 forming a three-dimensional silico-aluminate framework, which agreed with previous
234 observations of aluminosilicate-based geopolymers (Garcia-Lodeiro et al., 2015) (Davidovits
235 and Cordi, 1979). The presence of AlO₄(4Si) indicated that the concentration of charge-
236 balancing cations was sufficient to balance the negative charge of AlO₄ on the bridging oxygen
237 atoms in Si-O-Al linkages (Murdoch et al., 1985) (Perez-Cortes and Escalante-Garcia, 2020).
238 Variations in the H₂O/Na₂O ratio induced notable differences in the ²⁷Al spectra. The
239 predominant peak was observed at 58 ppm associated with Al q⁴(4Si) in the reaction products,
240 but a significant spectral intensity was also observed below 40 ppm (Al^V and Al^{VI} signals),
241 indicating that the unreacted metakaolin content increased with the H₂O/Na₂O ratio.



242



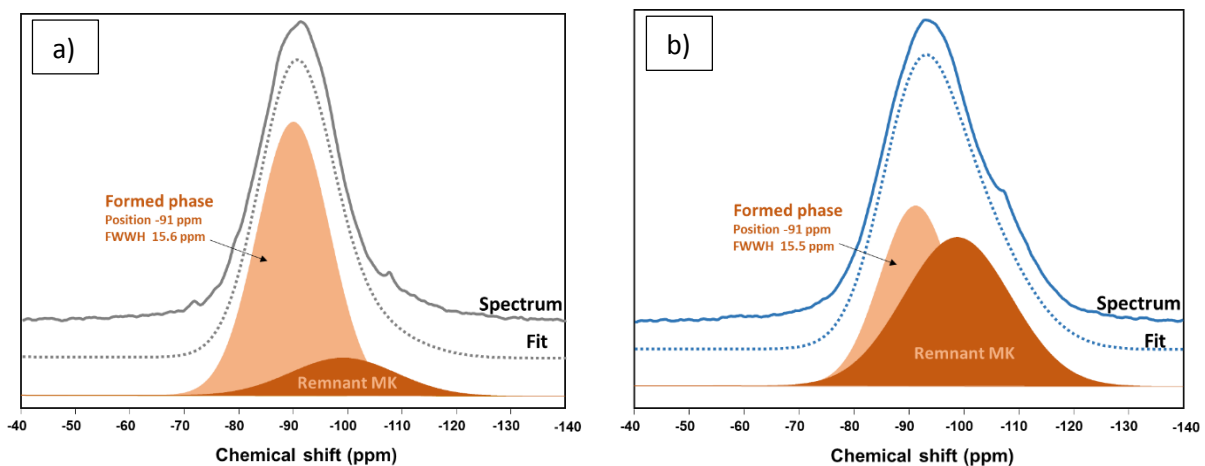
243

244

Figure 1 ^{27}Al spectra and ^{29}Si spectra of four mixtures and raw metakaolin

245 Regarding the ^{29}Si spectrum (Figure 1), the raw metakaolin spectrum presented an overall peak
246 with a maximum at approximately -101 ppm. This broad asymmetric resonance width indicated
247 the amorphous structure of the material. The peak detected at -107 ppm can be attributed to the
248 quartz present in raw metakaolin (Cherki El Idrissi et al., 2018a). The activated metakaolin
249 spectra shifted to higher frequencies, indicating structural changes in the short-ordered range.
250 The broad width indicated the presence of Si in different environments of type $\text{Q}^4(\text{mAl})$, where
251 m is the number of aluminum atom neighbors ($0 \leq m \leq 4$).

252 The ^{29}Si spectra were decomposed using Dmfit (Massiot et al., 2002) to form a phase and a
253 signal representing the remnant metakaolin (Figure 2). The decomposition results are presented
254 in Table 3.



255

256 **Figure 2** Decomposition of ^{29}Si MAS NMR spectra for a) MK21 and b) MK34 at 28 days

257 A difference was observed in the peak positions of the activated mixtures (Figure 1). For
258 mixtures MK21 and MK24, ^{29}Si resonance appeared at -91 ppm, whereas it appeared at slightly
259 higher frequencies (around -93 ppm) as $\text{H}_2\text{O}/\text{Na}_2\text{O}$ increased at 7 days. This variation in the
260 peak position was only an apparent shift, as it characterized the signal induced by unreacted

261 metakaolin overlapping with that of the geopolymer. The higher the water content, the higher
 262 the unreacted metakaolin, which resulted in varying positions of the overall peak (Table 3).

263 **Table 3 Analysis of ^{29}Si NMR spectra**

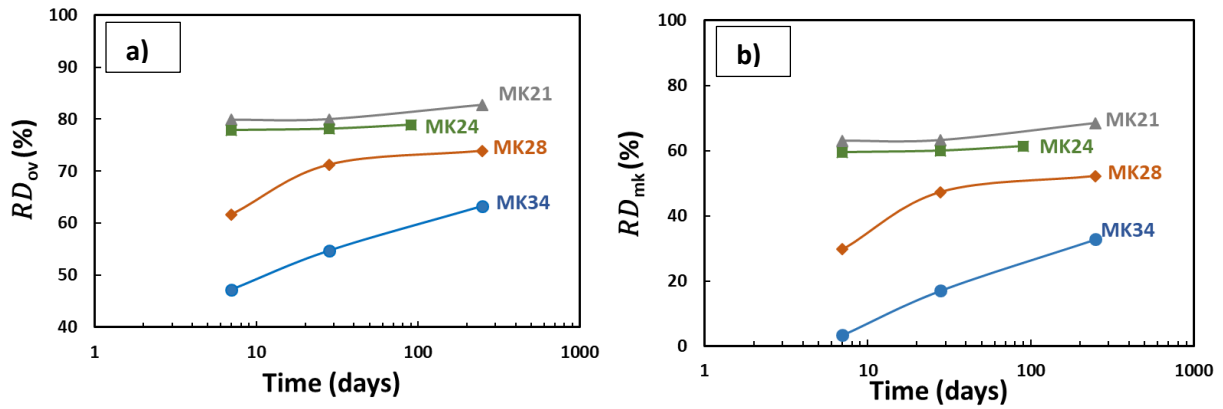
Mixtures		Remnant metakaolin	Formed phase		
		mol-%Si	Position (ppm)	FWHH	mol-%Si
MK21	7 days	20	-90.0	15.5	80
	28 days	20	-90.9	15.6	80
	250 days	17	-90.7	15.2	83
MK24	7 days	22	-91.3	15.6	78
	28 days	21	-91.3	15.1	79
	90 days	21	-90.7	15	79
MK28	7 days	38	-89.9	15.1	62
	28 days	29	-91.0	15.4	71
	250 days	26	-91.1	15.1	74
MK34	7 days	53	-91.5	15.8	47
	28 days	45	-91.1	15.5	55
	250 days	37	-91.4	16	63

264

265 The lower concentration of alkaline activator at high $\text{H}_2\text{O}/\text{Na}_2\text{O}$ content presumably resulted
 266 in a lower dissolution of silicates and aluminates from the raw material, resulting in fewer SiO_4
 267 and AlO_4 tetrahedral units to form a geopolymer gel. It was reported that increasing $\text{H}_2\text{O}/\text{Na}_2\text{O}$
 268 and $\text{Na}_2\text{O}/\text{Al}_2\text{O}_3$ tended to favor the formation of amorphous gel and various types of zeolites
 269 such as sodalite and zeolite belonging to the faujasite group, as well as zeolites X and A
 270 (Juengsuwattananon et al., 2019; Juengsuwattananon and Pimraksa, 2017). Other authors have
 271 suggested that high water content accelerates the rate of hydrolysis in systems with high Na_2O
 272 content resulting in the construction of nanocrystalline zeolite phases bound with

273 aluminosilicate gels (Zuhua et al., 2009). However, the formation of zeolitic structures or
274 geopolymers significantly depends on the initial molar ratio, which influences the strength. The
275 formation of zeolitic structures provides low-strength materials, whereas the formation of
276 geopolymeric structures provides high-strength materials (Juengsuwattananon et al., 2019). A
277 study reported that an amorphous geopolymeric phase was formed in samples with a higher
278 initial molar ratio of $\text{SiO}_2/\text{Al}_2\text{O}_3$ (3.0–4.0) with $\text{Na}_2\text{O}/\text{Al}_2\text{O}_3$ (1.0) and $\text{H}_2\text{O}/\text{Na}_2\text{O}$ ratios in the
279 range of 10.0–15.0; however, the study was limited to a $\text{H}_2\text{O}/\text{Na}_2\text{O}$ ratio of 20
280 (Juengsuwattananon et al., 2019). In addition, the ^{29}Si NMR results did not exhibit any sharp
281 peaks of different silicon environments associated with high ordering, which is typical for
282 zeolite structures (Buchwald, 2011). Therefore, increasing the $\text{H}_2\text{O}/\text{Na}_2\text{O}$ ratio in the range of
283 21–34 while maintaining the other molar ratios constant would not change the type of product.

284 The overall reaction degree RD_{ov} (calculated using Equation 2) and reaction degree R_{mk}
285 (calculated using Equation 3) are presented in **Figure 3** for all mixtures. The time evolution of
286 the reaction degree depended on the $\text{H}_2\text{O}/\text{Na}_2\text{O}$ ratio. At $\text{H}_2\text{O}/\text{Na}_2\text{O}$ ratios of 21 and 24, the
287 degree of reaction nearly stabilized after 7 days, whereas at higher ratios, the degree of reaction
288 significantly increased between 7 and 250 days. From an NMR perspective, this shows that a
289 higher amount of water delays the dissolution of the precursor without blocking the reaction
290 progress. A significant amount of the amorphous fraction of metakaolin did not react even under
291 highly alkaline conditions, as shown by R_{mk} . This amount of unreacted metakaolin could be
292 explained by the formation of a barrier layer of aluminosilicate gel on the surface of metakaolin,
293 which is likely to occur in mixtures activated by a silicate solution (Chen et al., 2017).



294

295 *Figure 3 Reaction degree as a function of time calculated from ²⁹Si NMR spectroscopy*

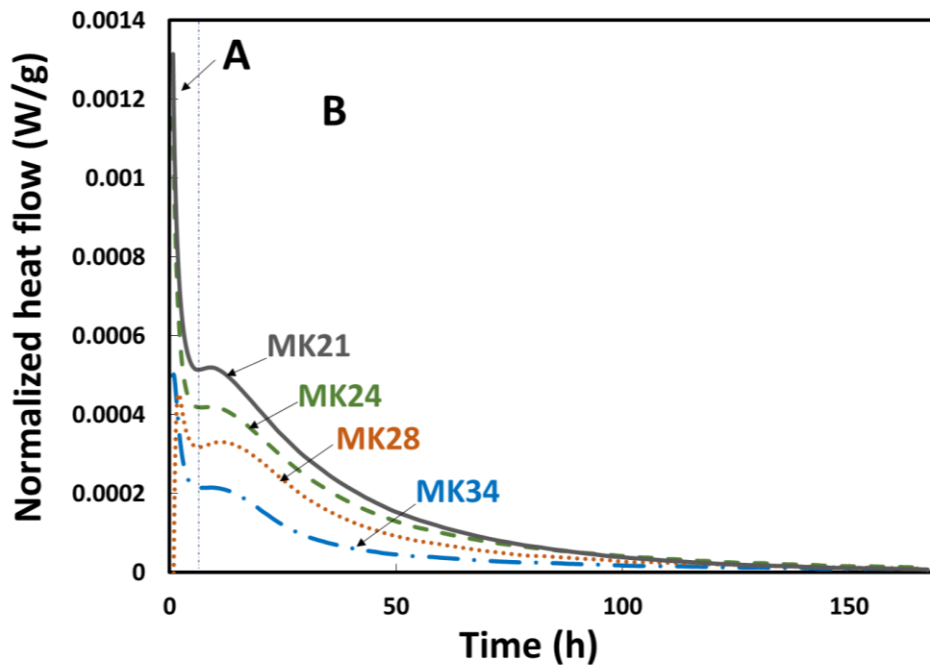
296

297 **3.1.2. Evolution of reaction degree**

298 The heat flux released per unit weight of the material is shown in Figure 4. The first peak can

299 be attributed to the heat release caused by the wetting and dissolution of metakaolin particles,

300 which is defined as stage A.



301

302 **Figure 4 Effect of water on heat flow per mass of material**

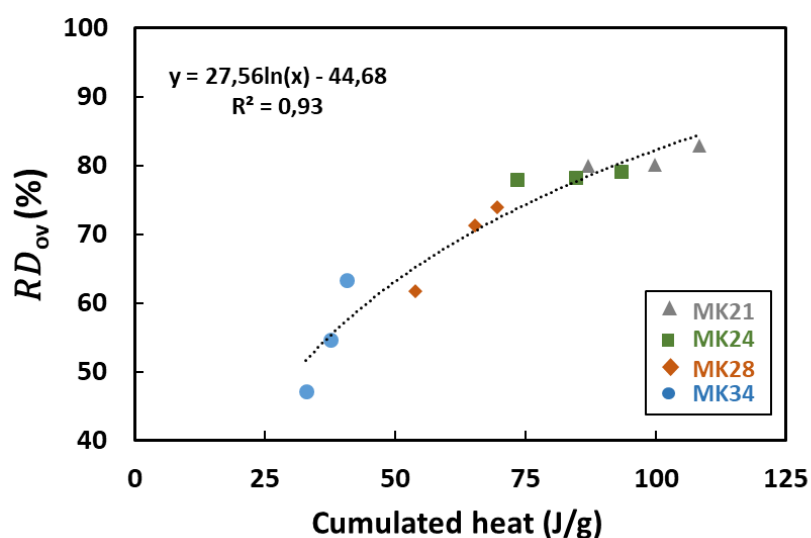
303 This peak decreased with increasing $\text{H}_2\text{O}/\text{Na}_2\text{O}$ ratios. After this stage, a second peak appeared
304 at approximately 10 and 12 h for all mixtures, with a slight shift in time as $\text{H}_2\text{O}/\text{Na}_2\text{O}$ increased.
305 At a high pH, the dissolution of amorphous aluminosilicate was fast and rapidly created a
306 supersaturated aluminosilicate solution. Oligomers were then formed and polycondensated into
307 a three-dimensional system (stage B). These two stages of the geopolymerization process have
308 been distinguished for a metakaolin-based material activated with sodium silicate solution
309 (Zhang et al., 2013). After 100 h, the evolution enters a thermally steady stage, during which
310 larger networks are formed by local reorganization.

311 During the first stage (A), hydroxide ions provided by the activation solution are assumed to
312 ensure the dissolution of the aluminosilicate source and the ionization of aluminate and silicate
313 monomers (Poulesquen et al., 2011). A low-modulus $\text{SiO}_2/\text{Na}_2\text{O}$ ratio of the sodium silicate
314 activator is known to favor a high degree of geopolymerization; however, its influence on the
315 first peak is less clear (Zhang et al., 2013).

316 In this study, the Na/Al ratio and activator modulus were kept constant; moreover, the increase
317 in the $\text{H}_2\text{O}/\text{Na}_2\text{O}$ ratio might favor the dissolution of the initial solid phases owing to higher
318 concentration gradients and faster diffusion. Thus, the magnitude of the heat flux during the
319 first stage was not affected. However, the intensity of the first peak decreased significantly with
320 increasing $\text{H}_2\text{O}/\text{Na}_2\text{O}$ ratio (Figure 4). This suggests that the dissolution of the precursor and
321 the extent of reaction are influenced, on the one hand, by the available surface of metakaolin
322 exposed to alkaline solution, which in turn is related to the metakaolin content (Favier et al.,
323 2013). On the other hand, it depends on the number of free hydroxides available to dissolve the
324 metakaolin phase (Benavent et al., 2016b). The total NaOH content decreased with increasing
325 water-to-solid ratio (Table 2). Consequently, the intensity of stage A is affected by the variation
326 in the $\text{H}_2\text{O}/\text{Na}_2\text{O}$ ratio. During the polymerization stage, the rate of polycondensation decreases
327 with increasing water content. Yao et al. (Yao et al., 2009) also observed this variation in heat

328 flux with an increase in the water content of NaOH-activated metakaolin. Another study (Zuhua
329 et al., 2009) demonstrated that a higher water-to-solid ratio accelerated the dissolution and
330 hydrolysis but hindered the polycondensation. Increasing the water content while maintaining
331 other ratios constant resulted in a decrease in the exothermic peak observed in the
332 polycondensation stage with a slight shift in time.

333 The degree of reaction at 7, 28, and 250 days (determined from NMR spectra) was plotted as a
334 function of the cumulative heat obtained using isothermal calorimetry for all mixtures (Figure
335 5). The cumulative heat at 28 and 250 days was determined through extrapolation using the $1/\sqrt{t}$
336 function (Lenormand et al., 2015). The degree of reaction followed a monotonically increasing
337 trend with respect to cumulative heat. This illustrates the correlation between the analyses
338 enabled by the different characterization techniques at the chemical level. The formation of the
339 main reaction product can be directly related to the heat released and can be monitored by
340 exothermic reactions. The decrease in the heat flow observed in the calorimetry curves can be
341 attributed to the lower reaction degree of the activated metakaolin mixture.



342

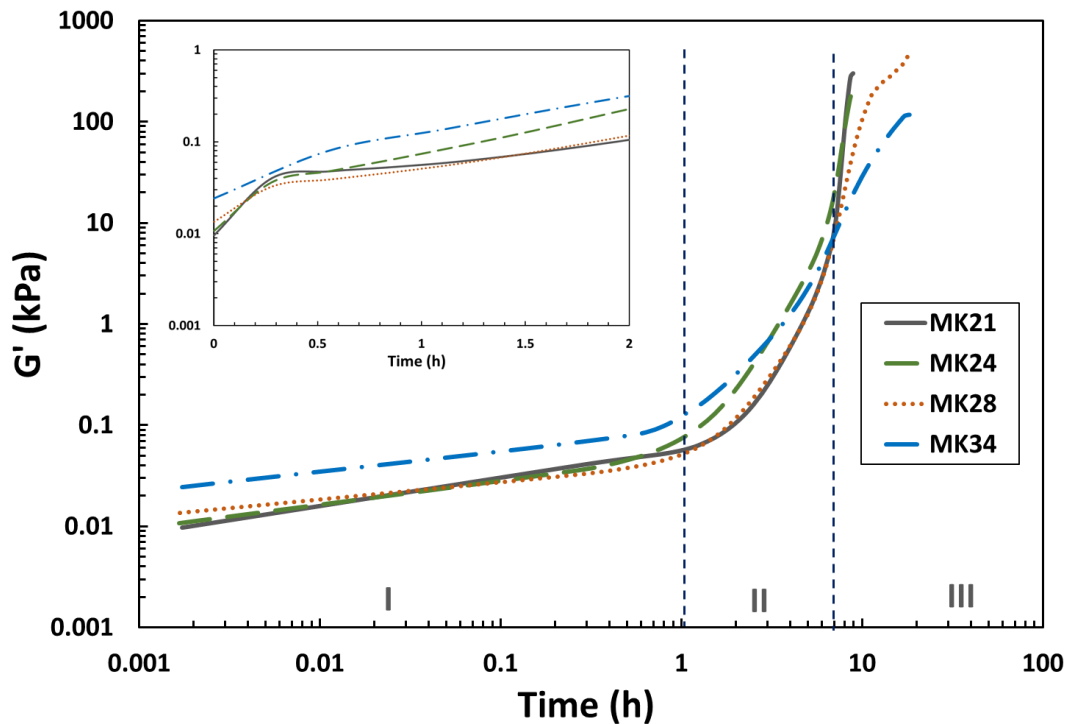
343

Figure 5 Reaction degree and cumulated heat

344 **3.2.Mechanical characterization**

345 **3.2.1. Rheological measurement**

346 The evolution of G' in the fresh state was plotted against time on a logarithmic scale for a better
347 understanding of the effect of water in the very early stages (Figure 6). G' evolved through
348 three main stages (I, II, and III in Figure 6). The first stage presents a constant growth rate, and
349 the second stage corresponds to an increasing rate of G' for all studied mixtures. The growth
350 rate during the third stage depends on the H_2O/Na_2O ratio. The elastic modulus of the mixture
351 MK21 increased rapidly and reached relatively high values within a short time. In contrast, the
352 mixture MK34 exhibited a slow increase in the elastic modulus and then stabilized at a low
353 value of 22 kPa. Variations in the elastic modulus suggested the formation of a more rigid
354 network in MK21 than in MK34. At high water-to-solid ratios, an increase in the amount of
355 water slowed the development of mechanical percolation paths. For a given reaction degree,
356 the distance between the aluminosilicate oligomers increased, and the number of mechanical
357 percolation paths decreased. A significant volume of product is required to reach the percolation
358 threshold, resulting in a lower elastic modulus (Stefan et al., 2010). Therefore, the elastic
359 modulus remained relatively low.



360

361

Figure 6 Evolution of elastic modulus G' as a function of time

362 The development of the elastic modulus as a function of H_2O/Na_2O did not follow a clear trend.

363 Different combined mechanisms may explain the variations in elastic modulus. At the

364 beginning of the first stage, the initial value of the elastic modulus is inversely correlated with

365 the H_2O/Na_2O ratio. This observation is in accordance with the attribution of the first increase

366 in the elastic modulus to the Al-rich gel formed between MK particles. [Favier et al. \(2013\)](#)

367 demonstrated that the colloidal interactions occurring between metakaolin particles suspended

368 in the activating solution are negligible. In addition, they observed that only low-energy

369 interactions occurred between particles as a result of the early formation of a low Si/Al

370 aluminosilicate inter-particle gel. This Al-rich gel located at the grain boundaries is responsible

371 for the initial elastic modulus. In this study, a higher H_2O/Na_2O ratio first induced faster

372 development of the elastic modulus. The concentration of the activation solution influenced the

373 kinetics of the dissolution and diffusion of aluminates $[Al(OH)_4]^-$. Thus, we can infer that a

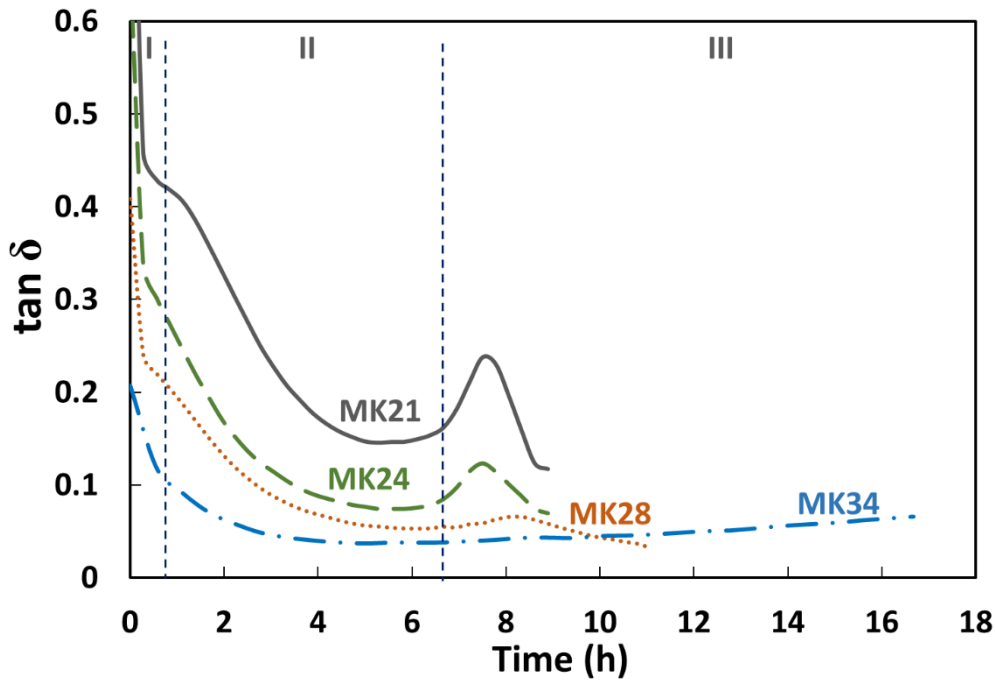
374 higher H_2O/Na_2O ratio enhances the dissolution and diffusion of aluminates at the beginning

375 of the first stage. Consequently, despite the high water content of these mixtures, the activation
376 solution enables the dissolution and hydrolysis processes to begin. In contrast, the dissolution
377 of $[\text{Al}(\text{OH})_4]^-$ depends on the exposed surface of metakaolin in contact with the alkaline solution
378 and the concentration of hydroxide ions, as mentioned earlier. Both the solid and liquid volume
379 fractions varied in these mixtures. Accordingly, the dissolution and diffusion of aluminate did
380 not follow a clear trend over time.

381 The mixture MK34 had the highest value of G' at a very early age. This can be attributed to the
382 easier formation of the Al-rich gel with a relatively low Si/Al ratio, as explained previously
383 (Favier et al., 2013). Another factor could be the reduced effect of the sodium silicate solution
384 (Romagnoli and Andreola, 2007). Anionic silicate oligomers present in alkaline solutions are
385 known to be highly efficient clay deflocculants, which probably increase the electrostatic
386 repulsion between particles and thus counteract attractive forces. Therefore, this effect may be
387 minimized in the mixture with a lower content of activation solution, and the amplification of
388 the elastic modulus is caused by the presence of particles, which dominate the system.

389 After a few hours, the curves intersected, and the magnitude of G' followed a different and
390 clearer trend ($G'_{21} > G'_{24} > G'_{28} > G'_{34}$). Thus, we can conclude that a new chemistry is
391 emerging, resulting in the formation of stiffer products. Favier et al. (Favier et al., 2013)
392 observed a decrease in Al concentration associated with an increasing growth rate of the elastic
393 properties. This suggests that aluminate reacts with silicate to form an aluminosilicate phase
394 with a higher Si/Al ratio.

395 The variation in $\tan \delta$ as a function of time is shown in Figure 7. First, $\tan \delta$ decreased because
396 G' varied more quickly than G'' , and it was always lower than 1 ($G' > G''$). A decrease in loss
397 factor can be attributed to the gradual gelation of the metakaolin geopolymer pastes (Rovnaník
398 et al., 2018). Subsequently, $\tan \delta$ went through a considerably constant stage. After a few hours,
399 $\tan \delta$ increased until it reached a peak value (Figure 7).



400

401

Figure 7 Evolution of $\tan \delta$ as a function of time

402 Several authors have mentioned that this peak presents a criterion of vitreous phase transition,
 403 which can be associated macroscopically with the gel time. Dai et al. (2020) explained this peak
 404 in the loss factor curve as the water released during the condensation reactions of the $\text{Si}(\text{OH})_4$
 405 species. After this peak, $\tan \delta$ gradually decreased, which may be due to the more indirect
 406 contact of particles, causing less loss of dissipated energy compared with more direct contact
 407 (Carreau, 2006). The rate of decrease in the loss factor after the peak was higher as the
 408 $\text{H}_2\text{O}/\text{Na}_2\text{O}$ ratio was lower. This could be attributed to a more elastic and rigid network with a
 409 low $\text{H}_2\text{O}/\text{Na}_2\text{O}$ ratio. For MK28, the time required to reach a stiffer state was longer than that
 410 for mixtures MK21 and MK24. The mixture MK34 had a steady stage in terms of the loss
 411 tangent.

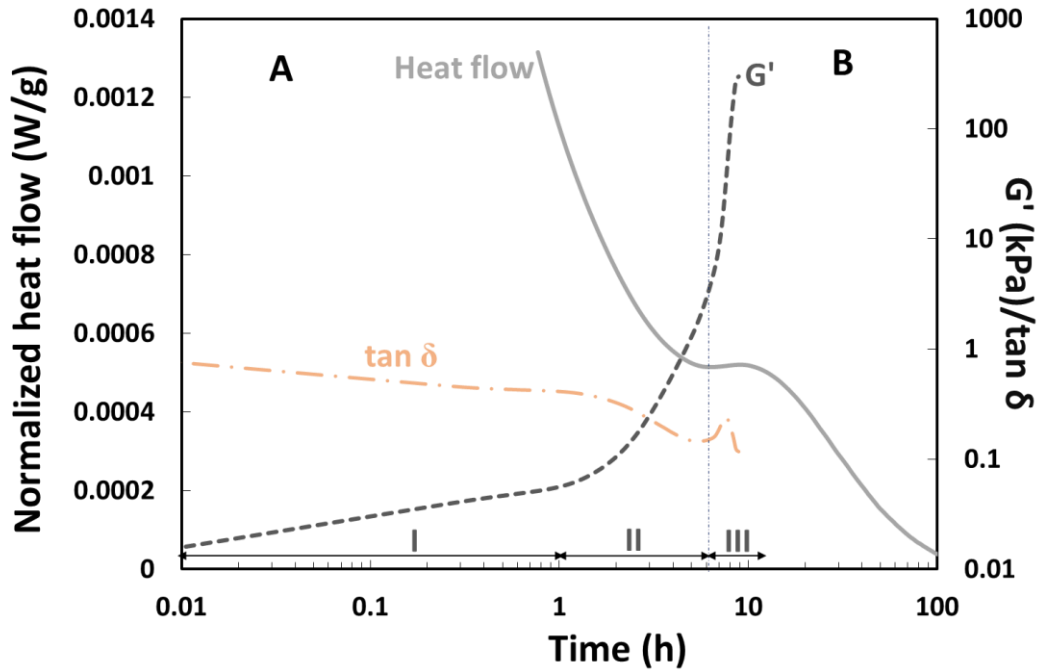
412 Moreover, lower water content resulted in higher $\tan \delta$ values ($\tan \delta_{21} > \tan \delta_{24} > \tan \delta_{28}$).

413 Normally, the $\tan \delta$ peak indicates that the dissipated energy exceeds the stored energy

414 associated with the interactions between the constituents. Oligomer polycondensation is the

415 origin of this phenomenon. A higher polycondensation rate is expected at a lower H₂O/Na₂O
416 ratio, which was evidenced by the higher value of the maximum tan δ in this study. Note that
417 MK34 did not harden during this period, which was consistent with the disappearance of the
418 maximum in the tan δ curve. This supported the assumption that the tan δ peak is associated
419 with the beginning of the development of the final geopolymer product. This implies that tan δ
420 can be a useful parameter for evaluating the effect of water on the magnitude of
421 geopolymerization reactions from the early stages.

422 Dynamic rheology and isothermal calorimetry were combined to analyze the influence of the
423 H₂O/Na₂O ratio on the behavior of fresh and hardened mixtures. G', tan δ , and heat release of
424 MK21 are plotted in Figure 8. After a linear increase in G', the first critical point appeared, and
425 the elastic modulus increased more rapidly but remained relatively low. The increase in G' may
426 be due to further dissolution of metakaolin particles and the formation of large oligomers. At
427 the beginning of stage B, a second critical point occurred, and the G' growth rate further
428 increased. During this stage, G' reached high values after a short time. The rapid increase in the
429 elastic modulus can be associated with the formation of large oligomers or the initiation of
430 polycondensation into a three-dimensional network, often called a geopolymer structure. These
431 critical points can be more easily distinguished for MK21 and MK24 mixtures than for MK28
432 and MK34.



433

434

Figure 8 Correlation between G' , $\tan \delta$, and heat flow for MK21

435 The second critical point of the different mixtures appeared at approximately the same time,
 436 but with different rate variations (Figure 6). This result suggested that all mixtures reached
 437 supersaturation simultaneously. This corresponded to a critical Si/Al ratio, which was
 438 consistent with the composition of the studied mixtures, as the Si/Al and Na/Al ratios were kept
 439 constant. The main difference between these mixtures was the water content. However, it has
 440 been demonstrated that water does not affect silicate species' condensation in alkaline silicate
 441 solutions (Bourlon, 2010). This agrees with the results of NMR spectroscopy (see Section
 442 3.1.1), which indicated that the local structure of the reaction products was not affected by the
 443 initial water content.

444 Consequently, the consistency between the evolution of the reaction rate and the evolution of
 445 the elastic modulus G' of the materials can be highlighted. An origin at the physicochemical
 446 level can be assumed. Studies have shown that an increase in the consumption of metakaolin is
 447 accompanied by an increase in the shear modulus of geopolymers. Similarly, the stabilization

448 of the consumption rate of metakaolin corresponds to the setting of the geopolymer (Bourlon,
449 2010).

450 **3.2.2. Correlations between mechanical properties and chemical reaction degree**

451 The compressive strength was measured at 7, 28, and 90 d for all mixtures except MK34. Its
452 compressive strength was lower than 25 kPa after 90 days, which corresponded to the minimum
453 compressive strength measurable by the machine on cylindrical specimens.

454 Table 4 lists the heat released, compressive strength, and water porosity at different ages. The
455 cumulative heat at 7 days was directly deduced from the experimental data of isothermal
456 calorimetry (Figure 4), and the cumulative heat at 28 days was determined by extrapolation
457 using the $1/\sqrt{t}$ function (Lenormand et al., 2015). The compressive strengths of all mixtures
458 primarily developed within the first 7 days. From the values at 7 and 28 days, the strength
459 development was not proportional to the cumulative released heat. Mixtures MK21 and MK24
460 had nearly the same cumulative heat at 7 and 28 days, but they exhibited significantly different
461 values of compressive strength. Thus, the data from calorimetry were not sufficient to explain
462 the development of strength, particularly the decrease in strength owing to the increase in the
463 H_2O/Na_2O ratio from 21 to 28. This confirms that strength development also depends on the
464 physical and microstructural parameters of the material. Thus, the water porosities at 28 and 90
465 days were also determined.

466 The porosity of the hardened material was proportional to the initial water content (Table 4).
467 This means that the pores replaced the main part of the initial water volume in the hardened
468 material, which was consistent with a previous study (Pouhet et al., 2019). Studies show that
469 the amount of water in the initial geopolymer system is the dominant factor affecting the density
470 and open porosity after extended aging (Benavent et al., 2016a; Lizcano et al., 2012). This
471 influence of porosity on strength is a priori similar to the behavior of ceramics, as the strength

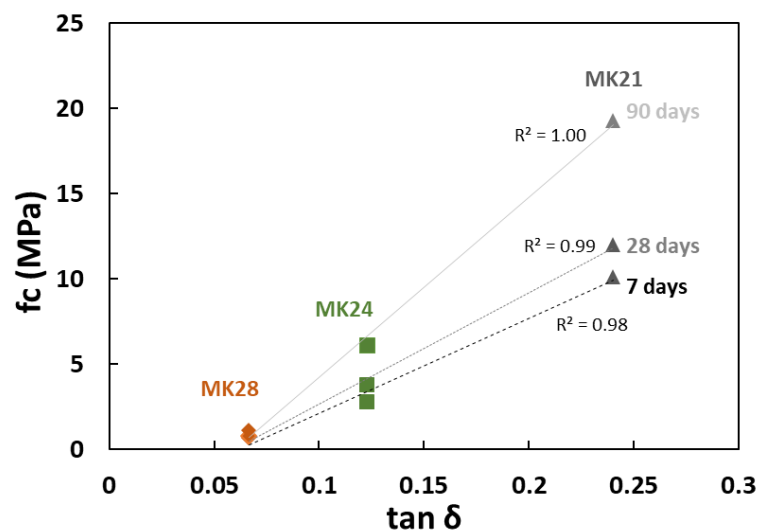
472 exponentially decreases with porosity (Kingery et al., 1976) (Biswas, 1976). The literature
 473 indicates that maintaining an H₂O/Na₂O ratio between 10 and 20 is necessary to achieve
 474 significant strength for a structural geopolymer (Cui, 2019). From the experimental results, a
 475 higher value of this ratio can enable the performance required for different applications to be
 476 attained, where high strength is not the main interest, provided that the materials exhibit the
 477 expected values of elastic modulus, water permeability, fire resistance, etc. A decrease in the
 478 strength and geopolymer content (Figure 9) was observed at approximately H₂O/Na₂O = 30.

479 A significant increase in the compressive strength occurred between 28 and 90 days, as shown
 480 in Table 4. However, the reaction degree of MK21, MK24, and MK28 mixtures did not
 481 significantly increase during this period (Figure 3). The porosity slightly decreased between 28
 482 and 90 days, which may partially explain the increase in the compressive strength. The
 483 refinement of the porosity of an activated metakaolin over time was attributed to the
 484 densification of the solid network and partial closure of the porosity at the nanometer scale
 485 (Steins et al., 2014). Moreover, a dissolution–precipitation mechanism occurring at the pore
 486 wall interface was observed, which could explain the slight decrease in the pore volume
 487 (Benavent et al., 2016a).

488 **Table 4 Released heat, compressive strength, and porosity after different ages**

Age (days)	Initial water (% vol)	Porosity (% vol.)		Released heat (J/g)		Compressive strength (MPa)		
		28	90	7	28	7	28	90
MK21	66	60.3	59.7	87.1	100	10.1	12.0	19.3
MK24	68	64.0	62.9	72.1	84.9	2.7	3.8	6.0
MK28	72	68.8	68.2	59.0	65.5	0.7	0.8	1.1
MK34	76	-	-	32.9	37.6	< 0.025	< 0.025	< 0.025

489 The compressive strength was plotted as a function of $\tan \delta$ obtained from rheological
 490 measurements (Figure 9). The maximum $\tan \delta$ obtained by rheological testing is linearly
 491 correlated with the compressive strength at 7, 28, and 90 days. This correlation between the
 492 mechanical properties at an early age and long-term results from multiple parameters, such as
 493 the reaction degree, microstructure parameters, and their time evolution. [Steins et al. \(2012\)](#)
 494 mentioned that the variation in the value of $\tan \delta$ is difficult to explain. As a word of caution
 495 before generalizing this correlation, note that it strongly depends on the material composition
 496 and examined objectives. In addition, MK34 did not develop significant mechanical strength
 497 even after 90 days, which was consistent with the disappearance of the maximum $\tan \delta$ for this
 498 mixture.



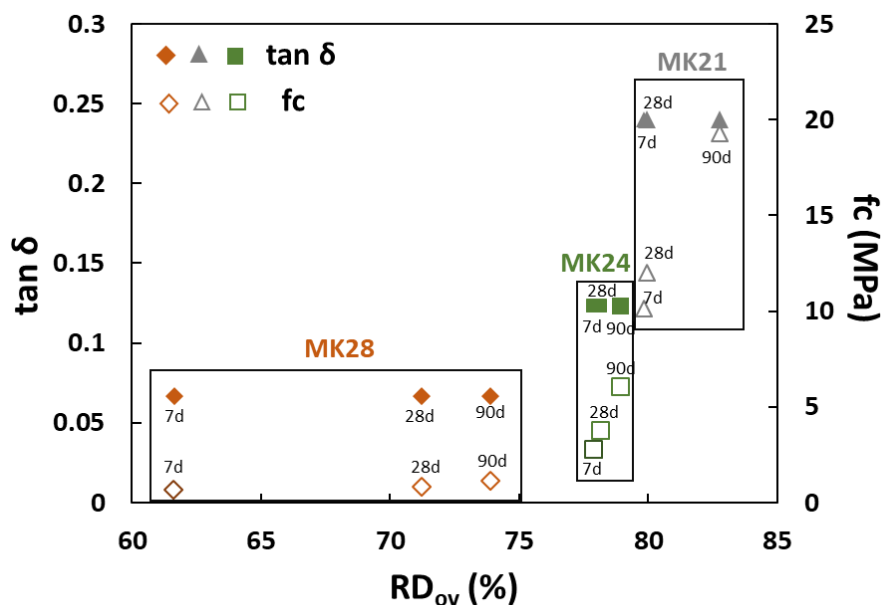
499

500 **Figure 9 Compressive strength as a function of the maximum of $\tan \delta$**

501 Finally, the compressive strength and maximum $\tan \delta$ are plotted as a function of the degree of
 502 reaction in Figure 10. A decrease in compressive strength was observed with an increase in the
 503 H_2O/Na_2O ratio. It has been reported that the compressive strength is linearly correlated with
 504 the reaction degree (Chen et al., 2020). However, in this study, the compressive strength was
 505 not correlated with the degree of reaction. MK21 and MK24 exhibited similar reaction degrees
 506 but developed different compressive strengths. Conversely, the significant increase in the

507 reaction degrees from MK28 to MK24 resulted in limited strength development. Both strength
 508 and $\tan \delta$ can be considered mechanical parameters. For instance, $\tan \delta$ was deduced from the
 509 G' values, which also sharply decreased with the H_2O/Na_2O ratio (Figure 6). The strength and
 510 $\tan \delta$ depend on the chemical reactivity of the binder, but not directly, as they are also influenced
 511 by the initial porosity and packing density of the mixture, the development of percolation paths,
 512 the intrinsic mechanical properties of each phase, and their complex interactions that influence
 513 the time evolution of the microstructure.

514 Based on this, $\tan \delta$ appears to be a useful parameter to anticipate the influence of the H_2O/Na_2O
 515 ratio on strength from short-term rheological measurements, and the correlation with strength
 516 enables us to understand its evolution.



517

518 *Figure 10 Compressive strength and $\tan \delta$ versus the degree of reaction*

519 **4. Conclusions**

520 [Metakaolin-based geopolymers were characterized using advanced experimental and analytical](#)
 521 [techniques to monitor the reaction advancement and development of mechanical properties](#)

522 from the fresh to the hardened state. The mixtures were designed by keeping the molar ratios
523 constant, only the H₂O/Na₂O ratio varied from 21 to 34. The following conclusions were drawn:

- 524 • The analysis of the phase composition suggested that water did not affect the structure
525 of the geopolymer-type phase. A higher H₂O/Na₂O ratio resulted in a higher content of
526 unreacted metakaolin and a lower product fraction, as shown by the NMR results.
- 527 • The combination of isothermal calorimetry and dynamic rheology allows to distinguish
528 the different stages of the structuration of fresh and hardening materials.
- 529 • The maximum loss tangent $\tan \delta$ appeared to be a reliable indicator for estimating the
530 sensitivity of the strength of the studied mixtures to the initial water content.
- 531 • At the chemical mechanism level, a correlation between the cumulated released heat
532 obtained by isothermal calorimetry and the degree of reaction deduced from the
533 decomposition of NMR spectra was revealed.
- 534 • The maximum $\tan \delta$ obtained using the rheological test was linearly correlated with the
535 compressive strength. The degree of reaction and mechanical properties were poorly
536 correlated at the studied scales of time and space. The decrease in compressive strength
537 with H₂O/Na₂O ratio was explained by the influence of water on the reactivity of the
538 precursor and the higher porosity of the material, as the water was not chemically bound.

539 **References**

- 540 Aboulayt, A., Jaafri, R., Samouh, H., Cherki El Idrissi, A., Roziere, E., Moussa, R., Loukili,
541 A., 2018. Stability of a new geopolymer grout: Rheological and mechanical
542 performances of metakaolin-fly ash binary mixtures. *Construction and Building*
543 *Materials* 181, 420–436. <https://doi.org/10.1016/j.conbuildmat.2018.06.025>
- 544 Aboulayt, A., Souayfan, F., Roziere, E., Jaafri, R., Cherki El Idrissi, A., Moussa, R., Justino,
545 C., Loukili, A., 2020. Alkali-activated grouts based on slag-fly ash mixtures: From
546 early-age characterization to long-term phase composition. *Construction and Building*
547 *Materials* 260, 120510. <https://doi.org/10.1016/j.conbuildmat.2020.120510>
- 548 Benavent, V., Frizon, F., Poulesquen, A., 2016a. Effect of composition and aging on the porous
549 structure of metakaolin-based geopolymers. *J Appl Crystallogr* 49, 2116–2128.
550 <https://doi.org/10.1107/S1600576716014618>
- 551 Benavent, V., Steins, P., Sobrados, I., Sanz, J., Lambertin, D., Frizon, F., Rossignol, S.,
552 Poulesquen, A., 2016b. Impact of aluminum on the structure of geopolymers from the

553 early stages to consolidated material. *Cement and Concrete Research* 90, 27–35.
554 <https://doi.org/10.1016/j.cemconres.2016.09.009>

555 Biswas, D.R., 1976. Influence of porosity on the mechanical properties of lead zirconate--
556 titanate ceramics (No. LBL-5479, 7110774). <https://doi.org/10.2172/7110774>

557 Bourlon, A., 2010. Physico-chimie et rhéologie de géopolymères frais pour la cimentation des
558 puits pétroliers, in french (PhD thesis). Université Paris VI.

559 Bruno, S., Claude, P., Laurent, B., Philippe, L., 2018. Amélioration et renforcement des sols -
560 AMSOL - Tome 2, in french, LE MONITEUR. ed.

561 Buchwald, A., 2011. Condensation of aluminosilicate gels—model system for geopolymer
562 binders. *Journal of Non-Crystalline Solids* 7.
563 <https://doi.org/10.1016/j.jnoncrysol.2010.12.036>

564 Carreau, P.J., 2006. Philippe Coussot: Rheometry of Pastes, Suspensions and Granular
565 Materials. Applications in Industry and Environment: JohnWiley and Sons, Inc.,
566 Hoboken, New Jersey. ISBN 0-471-65369-1, 291 pages, US \$89.95. *Rheol Acta* 46,
567 317–318. <https://doi.org/10.1007/s00397-006-0118-y>

568 Chen, X., Kim, E., Suraneni, P., Struble, L., 2020. Quantitative Correlation between the Degree
569 of Reaction and Compressive Strength of Metakaolin-Based Geopolymers. *Materials*
570 13, 5784. <https://doi.org/10.3390/ma13245784>

571 Chen, X., Sutrisno, A., Zhu, L., Struble, L.J., 2017. Setting and nanostructural evolution of
572 metakaolin geopolymer. *J Am Ceram Soc* 100, 2285–2295.
573 <https://doi.org/10.1111/jace.14641>

574 Cherki El Idrissi, A., 2019. The development of a global mix design and analysis approach for
575 alkali activated soil reinforcement grouts. *European Journal of Environmental and Civil*
576 *Engineering* 23, 645–656. <https://doi.org/10.1080/19648189.2018.1519461>

577 Cherki El Idrissi, A., Paris, M., Rozière, E., Deneele, D., Darson, S., Loukili, A., 2018a. Alkali-
578 activated grouts with incorporated fly ash: From NMR analysis to mechanical
579 properties. *Materials Today Communications* 14, 225–232.
580 <https://doi.org/10.1016/j.mtcomm.2018.01.012>

581 Cherki El Idrissi, A., Roziere, E., Loukili, A., Darson, S., 2018b. Design of geopolymer grouts:
582 the effects of water content and mineral precursor. *European Journal of Environmental*
583 *and Civil Engineering* 22, 628–649. <https://doi.org/10.1080/19648189.2016.1214183>

584 Clausi, M., Tarantino, S.C., Magnani, L.L., Riccardi, M.P., Tedeschi, C., Zema, M., 2016.
585 Metakaolin as a precursor of materials for applications in Cultural Heritage:
586 Geopolymer-based mortars with ornamental stone aggregates. *Applied Clay Science*
587 132–133, 589–599. <https://doi.org/10.1016/j.clay.2016.08.009>

588 Costa, L.M., Almeida, N.G.S., Houmard, M., Cetlin, P.R., Silva, G.J.B., Aguilar, M.T.P., 2021.
589 Influence of the addition of amorphous and crystalline silica on the structural properties
590 of metakaolin-based geopolymers. *Applied Clay Science* 215, 106312.
591 <https://doi.org/10.1016/j.clay.2021.106312>

592 Cui, Y., 2019. Effects of the n(H₂O_ Na₂Oeq) ratio on the geopolymerization process and
593 microstructures of fly ash-based geopolymers. *Journal of Non-Crystalline Solids* 10.
594 <https://doi.org/10.1016/j.jnoncrysol.2018.12.033>

595 Dai, X., Aydin, S., Yardimci, M.Y., Lesage, K., de Schutter, G., 2020. Influence of water to
596 binder ratio on the rheology and structural Build-up of Alkali-Activated Slag/Fly ash
597 mixtures. *Construction and Building Materials* 264, 120253.
598 <https://doi.org/10.1016/j.conbuildmat.2020.120253>

599 Davidovits, J., Cordi, S.A., 1979. Synthesis of New High-Temperature Geo-Polymers for
600 Reinforced Plastics/Composites. *Annu. Pac. Tech. Conf. Tech. Disp* 4 151–154.

601 Duxson, P., Fernández-Jiménez, A., Provis, J.L., Lukey, G.C., Palomo, A., van Deventer, J.S.J.,
602 2007. Geopolymer technology: the current state of the art. *J Mater Sci* 42, 2917–2933.
603 <https://doi.org/10.1007/s10853-006-0637-z>

604 Etemadi, H., Afsharkia, S., Zinatloo- Ajabshir, S., Shokri, E., 2021. Effect of alumina
605 nanoparticles on the antifouling properties of polycarbonate- polyurethane blend
606 ultrafiltration membrane for water treatment. *Polym Eng Sci* 61, 2364–2375.
607 <https://doi.org/10.1002/pen.25764>

608 Favier, A., Habert, G., d’Espinose de Lacaillerie, J.B., Roussel, N., 2013. Mechanical properties
609 and compositional heterogeneities of fresh geopolymer pastes. *Cement and Concrete*
610 *Research* 48, 9–16. <https://doi.org/10.1016/j.cemconres.2013.02.001>

611 Favier, Aurélie, Hot, J., Habert, G., Roussel, N., 2013. RHEOLOGY OF GEOPOLYMER:
612 COMPARATIVE STUDY BETWEEN PORTLAND CEMENT AND METAKAOLIN
613 BASED GEOPOLYMER 8.

614 Gadkar, A., Subramaniam, K.V.L., 2019. An evaluation of yield and Maxwell fluid behaviors
615 of fly ash suspensions in alkali-silicate solutions. *Mater Struct* 52, 117.
616 <https://doi.org/10.1617/s11527-019-1429-7>

617 Garcia-Lodeiro, I., Palomo, A., Fernández-Jiménez, A., 2015. An overview of the chemistry of
618 alkali-activated cement-based binders, in: *Handbook of Alkali-Activated Cements,*
619 *Mortars and Concretes.* Elsevier, pp. 19–47.
620 <https://doi.org/10.1533/9781782422884.1.19>

621 Güllü, H., Al Nuaimi, M.M.D., Aytok, A., 2020. Rheological and strength performances of
622 cold-bonded geopolymer made from limestone dust and bottom ash for grouting and
623 deep mixing. *Bull Eng Geol Environ.* <https://doi.org/10.1007/s10064-020-01998-2>

624 Güllü, H., Cevik, A., Al-Ezzi, K.M.A., Gülsan, M.E., 2019. On the rheology of using
625 geopolymer for grouting: A comparative study with cement-based grout included fly
626 ash and cold bonded fly ash. *Construction and Building Materials* 196, 594–610.
627 <https://doi.org/10.1016/j.conbuildmat.2018.11.140>

628 Hassan, A., Arif, M., Shariq, M., 2019. Use of geopolymer concrete for a cleaner and
629 sustainable environment – A review of mechanical properties and microstructure.
630 *Journal of Cleaner Production* 223, 704–728.
631 <https://doi.org/10.1016/j.jclepro.2019.03.051>

632 Hwalla, J., Saba, M., Assaad, J.J., 2020. Suitability of metakaolin-based geopolymers for
633 underwater applications. *Mater Struct* 53, 119. [https://doi.org/10.1617/s11527-020-](https://doi.org/10.1617/s11527-020-01546-0)
634 [01546-0](https://doi.org/10.1617/s11527-020-01546-0)

635 Juengsuwattananon, K., Pimraksa, K., 2017. Variable factors controlling amorphous-zeolite
636 phase transformation in metakaolin based geopolymer. *Acta Metall Slovaca* 23, 378–
637 386. <https://doi.org/10.12776/ams.v23i4.1001>

638 Juengsuwattananon, K., Winnefeld, F., Chindaprasirt, P., Pimraksa, K., 2019. Correlation
639 between initial SiO₂/Al₂O₃, Na₂O/Al₂O₃, Na₂O/SiO₂ and H₂O/Na₂O ratios on phase
640 and microstructure of reaction products of metakaolin-rice husk ash geopolymer.
641 *Construction and Building Materials* 226, 406–417.
642 <https://doi.org/10.1016/j.conbuildmat.2019.07.146>

643 Kingery, W.D., Bowen, H.K., Uhlmann, D.R., 1976. *Introduction to ceramics*, Wiley. ed. New
644 York.

645 Lenormand, T., Rozière, E., Loukili, A., Staquet, S., 2015. Incorporation of treated municipal
646 solid waste incineration electrostatic precipitator fly ash as partial replacement of
647 Portland cement: Effect on early age behaviour and mechanical properties. *Construction*
648 *and Building Materials* 96, 256–269.
649 <https://doi.org/10.1016/j.conbuildmat.2015.07.171>

650 Leonelli, C., Romagnoli, M., 2015. Rheology parameters of alkali-activated geopolymeric
651 concrete binders, in: *Handbook of Alkali-Activated Cements, Mortars and Concretes*.
652 Elsevier, pp. 133–169. <https://doi.org/10.1533/9781782422884.2.133>

653 Liu, X., Jiang, J., Zhang, H., Li, M., Wu, Y., Guo, L., Wang, W., Duan, P., Zhang, W., Zhang,
654 Z., 2020. Thermal stability and microstructure of metakaolin-based geopolymer blended
655 with rice husk ash. *Applied Clay Science* 196, 105769.
656 <https://doi.org/10.1016/j.clay.2020.105769>

657 Lizcano, M., Gonzalez, A., Basu, S., Lozano, K., Radovic, M., 2012. Effects of Water Content
658 and Chemical Composition on Structural Properties of Alkaline Activated Metakaolin-
659 Based Geopolymers. *J. Am. Ceram. Soc.* 95, 2169–2177.
660 <https://doi.org/10.1111/j.1551-2916.2012.05184.x>

661 Mahdavi, K., Zinatloo-Ajabshir, S., Yousif, Q.A., Salavati-Niasari, M., 2022. Enhanced
662 photocatalytic degradation of toxic contaminants using Dy₂O₃-SiO₂ ceramic
663 nanostructured materials fabricated by a new, simple and rapid sonochemical approach.
664 *Ultrasonics Sonochemistry* 82, 105892. <https://doi.org/10.1016/j.ultsonch.2021.105892>

665 Massiot, D., Fayon, F., Capron, M., King, I., Le Calvé, S., Alonso, B., Durand, J.-O., Bujoli,
666 B., Gan, Z., Hoatson, G., 2002. Modelling one- and two-dimensional solid-state NMR
667 spectra: Modelling 1D and 2D solid-state NMR spectra. *Magn. Reson. Chem.* 40, 70–
668 76. <https://doi.org/10.1002/mrc.984>

669 Murdoch, J.B., Stebbins, J.F., Carmichael, I.S.E., 1985. High-resolution ²⁹Si NMR study of
670 silicate and aluminosilicate glasses: the effect of network-modifying cations. *American*
671 *Mineralogist* 70, 332–343.

672 NF EN 12390-1, 2012. Testing hardened concrete - Part 1 : shape, dimensions and other
673 requirements for specimens and moulds. AFNOR.

674 NF EN 12390-3, 2019. Testing hardened concrete - Part 3 : compressive strength of test
675 specimens. AFNOR.

676 NF P18-459, 2010. Concrete - Testing hardened concrete - Testing porosity and density.
677 AFNOR.

678 Panias, D., Giannopoulou, I.P., Perraki, T., 2007. Effect of synthesis parameters on the
679 mechanical properties of fly ash-based geopolymers. *Colloids and Surfaces A:
680 Physicochemical and Engineering Aspects* 301, 246–254.
681 <https://doi.org/10.1016/j.colsurfa.2006.12.064>

682 Perez-Cortes, P., Escalante-Garcia, J.I., 2020. Gel composition and molecular structure of
683 alkali-activated metakaolin-limestone cements. *Cement and Concrete Research* 13.
684 <https://doi.org/10.1016/j.cemconres.2020.106211>

685 Pouhet, R., Cyr, M., Bucher, R., 2019. Influence of the initial water content in flash calcined
686 metakaolin-based geopolymer. *Construction and Building Materials* 201, 421–429.
687 <https://doi.org/10.1016/j.conbuildmat.2018.12.201>

688 Poulesquen, A., Frizon, F., Lambertin, D., 2011. Rheological behavior of alkali-activated
689 metakaolin during geopolymerization. *Journal of Non-Crystalline Solids* 357, 3565–
690 3571. <https://doi.org/10.1016/j.jnoncrysol.2011.07.013>

691 Provis, J., 2013. Alkali activated materials: state-of-the-art report, RILEM TC 224-AAM,
692 Springer Science&Business Media. ed. Springer, New York.

693 Provis, J.L., 2014. Geopolymers and other alkali activated materials: why, how, and what?
694 *Mater Struct* 15. <https://doi.org/10.1617/s11527-013-0211-5>

695 Provis, J.L., Yong, C.Z., Duxson, P., van Deventer, J.S.J., 2009. Correlating mechanical and
696 thermal properties of sodium silicate-fly ash geopolymers. *Colloids Surf. A:
697 Physicochem. Eng. Asp* 57–63.

698 Rifaai, Y., Yahia, A., Mostafa, A., Aggoun, S., Kadri, E.-H., 2019. Rheology of fly ash-based
699 geopolymer: Effect of NaOH concentration. *Construction and Building Materials* 223,
700 583–594. <https://doi.org/10.1016/j.conbuildmat.2019.07.028>

701 Romagnoli, M., Andreola, F., 2007. Mixture of deflocculants: A systematic approach. *Journal*
702 *of the European Ceramic Society* 27, 1871–1874.
703 <https://doi.org/10.1016/j.jeurceramsoc.2006.05.065>

704 Rovnaník, P., Rovnaníková, P., Vyšvařil, M., Grzeszczyk, S., Janowska-Renkas, E., 2018.
705 Rheological properties and microstructure of binary waste red brick powder/metakaolin
706 geopolymer. *Construction and Building Materials* 188, 924–933.
707 <https://doi.org/10.1016/j.conbuildmat.2018.08.150>

708 Saak, A.W., Jennings, H.M., Shah, S.P., 2001. The influence of wall slip on yield stress and
709 viscoelastic measurements of cement paste. *Cement and Concrete Research* 31, 205–
710 212. [https://doi.org/10.1016/S0008-8846\(00\)00440-3](https://doi.org/10.1016/S0008-8846(00)00440-3)

711 San Nicolas, R., Cyr, M., Escadeillas, G., 2013. Characteristics and applications of flash
712 metakaolins. *Applied Clay Science* 83–84, 253–262.
713 <https://doi.org/10.1016/j.clay.2013.08.036>

714 Sathonsaowaphak, A., Chindapasirt, P., Pimraksa, K., 2009. Workability and strength of
715 lignite bottom ash geopolymer mortar. *Journal of Hazardous Materials* 168, 44–50.
716 <https://doi.org/10.1016/j.jhazmat.2009.01.120>

717 Scrivener, K., Martirena, F., Bishnoi, S., Maity, S., 2018. Calcined clay limestone cements
718 (LC3). *Cement and Concrete Research* 114, 49–56.
719 <https://doi.org/10.1016/j.cemconres.2017.08.017>

720 Souayfan, F., Rozière, E., Paris, M., Deneele, D., Loukili, A., Justino, C., 2022. 29Si and 27Al
721 MAS NMR spectroscopic studies of activated metakaolin-slag mixtures. *Construction*
722 *and Building Materials* 322, 126415.
723 <https://doi.org/10.1016/j.conbuildmat.2022.126415>

724 Stefan, L., Benboudjema, F., Torrenti, J.-Michel., Bissonnette, B., 2010. Prediction of elastic
725 properties of cement pastes at early ages. *Computational Materials Science* 47, 775–
726 784. <https://doi.org/10.1016/j.commatsci.2009.11.003>

727 Steins, P., Poulesquen, A., Diat, O., Frizon, F., 2012. Structural Evolution during
728 Geopolymerization from an Early Age to Consolidated Material. *Langmuir* 28, 8502–
729 8510. <https://doi.org/10.1021/la300868v>

730 Steins, P., Poulesquen, A., Frizon, F., Diat, O., Jestin, J., Causse, J., Lambertin, D., Rossignol,
731 S., 2014. Effect of aging and alkali activator on the porous structure of a geopolymer. *J*
732 *Appl Crystallogr* 47, 316–324. <https://doi.org/10.1107/S160057671303197X>

733 Turner, L.K., Collins, F.G., 2013. Carbon dioxide equivalent (CO₂-e) emissions: A comparison
734 between geopolymer and OPC cement concrete. *Construction and Building Materials*
735 43, 125–130. <https://doi.org/10.1016/j.conbuildmat.2013.01.023>

736 Weng, L., Sagoe-Crentsil, K., 2007. Dissolution processes, hydrolysis and condensation
737 reactions during geopolymer synthesis: Part I—Low Si/Al ratio systems. *J Mater Sci*
738 42, 2997–3006. <https://doi.org/10.1007/s10853-006-0820-2>

739 Wu, Y., Lu, B., Yi, Z., Du, F., Zhang, Y., 2019. The Properties and Latest Application of
740 Geopolymers. *IOP Conf. Ser.: Mater. Sci. Eng.* 472, 012029.
741 <https://doi.org/10.1088/1757-899X/472/1/012029>

742 Yaghoubi, M., Arulrajah, A., Disfani, M.M., Horpibulsuk, S., Darmawan, S., Wang, J., 2019.
743 Impact of field conditions on the strength development of a geopolymer stabilized
744 marine clay. *Applied Clay Science* 167, 33–42.
745 <https://doi.org/10.1016/j.clay.2018.10.005>

746 Yahya, Z., Abdullah, M., Hussin, K., Ismail, K., Razak, R., Sandu, A., 2015. Effect of Solids-
747 To-Liquids, Na₂SiO₃-To-NaOH and Curing Temperature on the Palm Oil Boiler Ash

748 (Si + Ca) Geopolymerisation System. *Materials* 8, 2227–2242.
749 <https://doi.org/10.3390/ma8052227>

750 Yang, J., Xu, L., Wu, H., Jin, J., Liu, L., 2022. Microstructure and mechanical properties of
751 metakaolin-based geopolymer composites containing high volume of spodumene
752 tailings. *Applied Clay Science* 218, 106412. <https://doi.org/10.1016/j.clay.2022.106412>

753 Yao, X., Zhang, Z., Zhu, H., Chen, Y., 2009. Geopolymerization process of alkali-
754 metakaolinite characterized by isothermal calorimetry. *Thermochimica Acta* 493, 49-
755 54. <https://doi.org/10.1016/j.tca.2009.04.002>

756 Zhang, B., Guo, H., Yuan, P., Li, Y., Wang, Q., Deng, L., Liu, D., 2020. Geopolymerization of
757 halloysite via alkali-activation: Dependence of microstructures on precalcination.
758 *Applied Clay Science* 185, 105375. <https://doi.org/10.1016/j.clay.2019.105375>

759 Zhang, B., Yuan, P., Guo, H., Deng, L., Li, Y., Li, L., Wang, Q., Liu, D., 2021. Effect of curing
760 conditions on the microstructure and mechanical performance of geopolymers derived
761 from nanosized tubular halloysite. *Construction and Building Materials* 268, 121186.
762 <https://doi.org/10.1016/j.conbuildmat.2020.121186>

763 Zhang, M., Zhao, M., Zhang, G., Nowak, P., Coen, A., Tao, M., 2015. Calcium-free
764 geopolymer as a stabilizer for sulfate-rich soils. *Applied Clay Science* 108, 199–207.
765 <https://doi.org/10.1016/j.clay.2015.02.029>

766 Zhang, Z., Provis, J.L., Wang, H., Bullen, F., Reid, A., 2013. Quantitative kinetic and structural
767 analysis of geopolymers. Part 2. Thermodynamics of sodium silicate activation of
768 metakaolin. *Thermochimica Acta* 565, 163–171.
769 <https://doi.org/10.1016/j.tca.2013.01.040>

770 Zinatloo-Ajabshir, S., Baladi, M., Salavati-Niasari, M., 2021. Sono-synthesis of MnWO₄
771 ceramic nanomaterials as highly efficient photocatalysts for the decomposition of toxic
772 pollutants. *Ceramics International* 47, 30178–30187.
773 <https://doi.org/10.1016/j.ceramint.2021.07.197>

774 Zinatloo-Ajabshir, S., Shafaati, E., Bahrami, A., 2022. Facile fabrication of efficient Pr₂Ce₂O₇
775 ceramic nanostructure for enhanced photocatalytic performances under solar light.
776 *Ceramics International* 48, 24695–24705.
777 <https://doi.org/10.1016/j.ceramint.2022.05.116>

778 Zuhua, Z., Xiao, Y., Huajun, Z., Yue, C., 2009. Role of water in the synthesis of calcined kaolin-
779 based geopolymer. *Applied Clay Science* 43, 218–223.
780 <https://doi.org/10.1016/j.clay.2008.09.003>

781

1 **Comprehensive study on the reactivity and mechanical properties of alkali-**
2 **activated metakaolin at high H₂O/Na₂O ratios**

3 Faten Souayfan^a, Emmanuel Roziere^a, Christophe Justino^b, Michaël Paris^c, Dimitri Deneele^{c,d},
4 Ahmed Loukili^a

5 ^a Civil engineering and Mechanics Research Institute (GeM), UMR-CNRS 6183, Ecole Centrale
6 de Nantes, 1 rue de la Noe – 44321 Nantes, France

7 ^b Soletanche-Bachy, Chemin des Processions – 77130 Montereau Fault Yonne, France

8 ^c Université de Nantes, CNRS, Institut des Matériaux Jean Rouxel, IMN, F-44000 Nantes,
9 France

10 ^d GERS-LGIE, Université Gustave Eiffel, IFSTTAR, F-44344 Bouguenais, France

11 **Abstract**

12 This study focused on the influence of high H₂O/Na₂O ratios (higher than 20) on the properties
13 of metakaolin-based geopolymers in fresh and hardened states while keeping constant Si/Al
14 and Na/Al atomic ratios. The increase in H₂O/Na₂O ratio from 21 to 34 resulted in a decrease
15 of 7-day compressive strength from 10 to 0.025 MPa. This can be attributed to the influence of
16 water on the reactivity of the precursor, which was demonstrated by nuclear magnetic resonance
17 (NMR) spectroscopy and porosity evolution as the water is not chemically bound. Increasing
18 H₂O/Na₂O ratio did not change the geopolymer structure of reaction products. A correlation
19 was observed between the reaction degree deduced from NMR spectral decomposition and the
20 cumulated released heat obtained using isothermal calorimetry. The maximum loss tangent,
21 obtained using dynamic rheology, was linearly related to strength development.

22 **Keywords:** Geopolymer, Metakaolin, Water content, Reaction degree, Mechanical properties,
23 Viscoelastic properties

24 **1. Introduction**

25 Geopolymer materials can be obtained by activating solid aluminosilicate sources under the
26 action of an alkaline solution at a high pH (Provis, 2014). Under these conditions, a precursor
27 is dissolved to enrich the medium with reactive monomers, followed by the orientation,
28 polycondensation, and formation of a three-dimensional rigid network (Provis, 2013). Calcined
29 clay containing metakaolin is a common aluminosilicate precursor used for geopolymer
30 formation (Liu et al., 2020; Yang et al., 2022; Zhang et al., 2021, 2020) . Among the different
31 options, kaolinitic clays are widely considered because of their availability (Scrivener et al.,
32 2018) and environmental impact (Turner and Collins, 2013). The alkaline activation of these
33 calcined clays results in the formation of a geopolymer structure (Cherki El Idrissi et al., 2018a;
34 Costa et al., 2021) (Garcia-Lodeiro et al., 2015) instead of hydration products with chemically
35 bound water. Therefore, geopolymers are considered a method to improve the technical
36 performance and sustainability of construction materials in different applications (Clausi et al.,
37 2016; Güllü et al., 2020; Hassan et al., 2019; Wu et al., 2019). Metakaolin-based geopolymers
38 are now being considered for civil engineering applications, including soil improvement and
39 the containment of polluted soils. These studies require the use of grouts, i.e. relatively diluted
40 mixtures, incorporated in existing soil. Here, a high strength is not the main requirement, but
41 low water permeability and high durability in potentially aggressive waters are expected
42 (Yaghoubi et al., 2019; Zhang et al., 2015).

43 Metakaolin-based geopolymers are expected to satisfy several specifications in fresh and
44 hardened states, depending on the intended application. For example, grouts used for soil
45 improvement with a high water-to-solid ratio should be stable during storage before use and
46 have relatively low viscosities, and these properties should be maintained during the entire
47 duration of the process (Aboulayt et al., 2020, 2018; Güllü et al., 2019). In structural
48 applications, mortar and concrete should be designed with workability and strength equivalent

49 to cement-based materials (Hassan et al., 2019). Therefore, independent of the application and
50 durability requirements, the rheology of a material in its fresh state is vital. Aboulayt et al.
51 (Aboulayt et al., 2018) demonstrated the ability of metakaolin grouts to satisfy different
52 specifications, including open time; however, they have a relatively high viscosity. The
53 relatively high specific surface area of metakaolin and the properties of sodium silicate
54 solutions (Gadkar and Subramaniam, 2019; Hwalla et al., 2020; San Nicolas et al., 2013) result
55 in high viscosity and poor workability, which limits its potential uses. The viscosity of
56 metakaolin geopolymers at low shear rates has been observed to depend on their solid content
57 (Leonelli and Romagnoli, 2015). (Favier et al., 2013) reported that the high viscosity of an
58 activated metakaolin binder is primarily controlled by the viscosity of the alkaline silicate
59 solution and not by the solid fraction, which explains why the common plasticizers used in the
60 concrete industry are not efficient in metakaolin-based geopolymers. Consequently, the mixture
61 proportions and associated ratios are key parameters for controlling the properties of
62 metakaolin-based geopolymers. Water content is a major parameter for controlling the
63 properties in the fresh state.

64 Additionally, in specific applications, such as deep soil mixing (Bruno et al., 2018), water is
65 considered a crucial parameter that affects the properties of hardened materials, even if high
66 strength is not required. When the grout is mixed with the soil, water from the soil is added to
67 the initial mixture; thus, the total water-to-solid ratio increases significantly. Thus, the influence
68 of high water content must be quantified to determine its influence in both fresh and hardened
69 states in highly diluted systems.

70 Water influences geopolymerization reactions as it is involved in dissolution, hydrolysis, and
71 polycondensation reactions (Weng and Sagoe-Crentsil, 2007). (Sathonsaowaphak et al., 2009)
72 reported that water is the only efficient lever for the workability of geopolymers. (Cherki El
73 Idrissi et al., 2018b) demonstrated that a high water content is required to achieve the expected

74 rheological properties of a metakaolin grout, but it may affect its mechanical properties. Other
 75 authors (Paniyas et al., 2007; Provis et al., 2009; Souayfan et al., 2022; Yahya et al., 2015) proved
 76 that water content is a crucial parameter in the synthesis of geopolymers for the development
 77 of mechanical strength.

78 **Table 1** lists the experimental conditions used in recent studies on the influence of water
 79 content. Cui (2019) demonstrated that a higher H₂O/Na₂O ratio in the range of 13–17
 80 contributes to the dissolution of the active component of the precursor but hinders the
 81 polymerization reaction of monomeric and oligomeric gels. Juengsuwattananon et al. (2019)
 82 correlated the phase structures of reaction products with different initial chemical compositions,
 83 including different H₂O/Na₂O ratios (from 10 to 20). Depending on the initial composition,
 84 zeolitic or geopolymer structures are formed, which directly affect strength development.

85 **Table 1. Comparison of this study with previous recent works on the influence of water**
 86 **content under different experimental conditions**

	(Juengsuwattananon et al., 2019)	(Pouhet et al., 2019)	(Cui, 2019)	Present study
H₂O/Na₂O	From 10 to 20	-	From 13 to 17	From 21 to 34
Na/Al-Si/Al	Variables	Variables	Constant	Constant
Water/solid ratio	From 0.51 to 1.5	From 0.35 to 0.75	-	From 0.65 to 1
Precursor	Metakaolin	Metakaolin	Fly ash class F	Metakaolin
State	Hardened material	Hardened material	Fresh and hardened material	Fresh and hardened material
Techniques	CS/SEM/XRD	CS/MIP/SEM/XRD/TGA	IC/XRD/FTIR/MIP/SEM/TGA/CS	IC/RMN/Dynamic rheology/Water porosity/CS

87 *CS: compressive strength; XRD: X-ray diffraction; SEM: scanning electron microscopy;
 88 TGA: thermogravimetric analysis; MIP: mercury intrusion porosimetry; IC: isothermal
 89 calorimetry; FTIR: Fourier-transform infrared spectroscopy

90 Pouhet et al. (2019) observed a linear decrease in the mechanical strength of a geopolymer and
91 reported that the major part of the initial water was not bonded to the structure. Thus, water not
92 only influences the rheological properties but also the advancement of the reaction, structure,
93 and strength of geopolymers. Therefore, a comprehensive study is necessary to understand the
94 features of nanostructures (Etemadi et al., 2021; Mahdavi et al., 2022; Zinatloo-Ajabshir et al.,
95 2022, 2021) to explain the properties at the macroscopic scale.

96 Few studies investigated the influence of water content independent of other parameters. Most
97 existing studies focused on the liquid-activator-to-solid-precursor and SiO_2 -to- Na_2O ratios.
98 Their variations influence the $\text{H}_2\text{O}/\text{Na}_2\text{O}$ ratio and other molar ratios. Therefore, predicting the
99 influence of water content on the behavior and engineering properties of metakaolin-based
100 geopolymers from fresh to hardened states is still difficult. It was reported that an $\text{H}_2\text{O}/\text{Na}_2\text{O}$
101 ratio between 10 and 20 is necessary to reach significant strength for a structural geopolymer
102 (Cui, 2019). High molar $\text{H}_2\text{O}/\text{Na}_2\text{O}$ ratios (higher than 20) can be expected to result in a tradeoff
103 between workability, mechanical properties, and durability, only a few investigations addressed
104 such high molar ratios, as shown in Table 1. Hence, a comprehensive study on the influence of
105 higher $\text{H}_2\text{O}/\text{Na}_2\text{O}$ ratios on short- and long-term properties, with controlled molar ratios, is
106 required.

107 Therefore, the main aim of this paper is to highlight the effects of the $\text{H}_2\text{O}/\text{Na}_2\text{O}$ ratio on the
108 reactivity and mechanical properties of metakaolin-based geopolymers to provide useful
109 information for the design of materials with different specifications. Several sodium silicate-
110 activated metakaolin mixtures were designed by varying $\text{H}_2\text{O}/\text{Na}_2\text{O}$ while maintaining constant
111 Si/Al and Na/Al atomic ratios. The effect of $\text{H}_2\text{O}/\text{Na}_2\text{O}$ is of primary importance in the design
112 of metakaolin-based geopolymers. This article provides a comprehensive study on the effect of
113 $\text{H}_2\text{O}/\text{Na}_2\text{O}$ and a base of knowledge on different techniques and combined approaches to
114 provide useful methodologies for further research. The behaviors of fresh and hardened

115 materials were investigated through isothermal calorimetry and dynamic rheology in the linear
116 viscoelastic range. Dynamic rheology provides deep insight into the evolution of the early
117 development of mechanical properties (Rifaai et al., 2019). The local structures of the hardened
118 grouts were investigated using nuclear magnetic resonance (NMR). The compressive strength
119 was determined at different ages and correlated to the maximum loss tangent ($\tan \delta$) obtained
120 using rheological tests and the degree of reaction calculated from NMR spectra decomposition.
121 The actual porosity was also assessed to understand the influence of the $\text{H}_2\text{O}/\text{Na}_2\text{O}$ ratio on
122 strength.

123

124 2. Experimental program

125 2.1. Materials and mixtures preparation

126 The studied mixtures were designed using metakaolin as a precursor and an activation solution
127 based on sodium silicate. Metakaolin was produced using the flash calcination of clay from
128 Fumel, France. The relatively high silica content of metakaolin (67.1 wt.%) was due to a
129 significant proportion of quartz. The proportion of the pure metakaolin $\text{Al}_2\text{O}_3(\text{SiO}_2)_2$ phase was
130 43 wt.%. The mass fractions of CaO, Fe_2O_3 , MgO, TiO_2 , and Na_2O were 1.1%, 2.6%, 0.11%,
131 1.3%, and 0.01%, respectively. The average particle size of metakaolin was 18 μm , its density
132 was 2.63, and its specific surface area was 16.5 m^2/g as determined using N_2 sorption and the
133 Brunauer–Emmett–Teller (BET) method.

134 The activation solution was prepared by diluting a sodium silicate solution with a fixed
135 $\text{SiO}_2/\text{Na}_2\text{O}$ ratio of 1.7 and a dry content of 44% in demineralized water. The sodium silicate
136 solution was specially designed with a relatively high Na_2O content to reduce the subsequent
137 addition of NaOH as much as possible during the preparation of the studied mixtures. A very
138 low NaOH content was added in pellets to adjust the Na/Al ratio to 1. The molar ratio of SiO_2
139 to Na_2O in the activator and the chemical composition was selected as recommended in the
140 literature to facilitate good dissolution of the precursor (Duxson et al., 2007).

141 Four mixtures were designed with constant Si/Al and Na/Al molar ratios and different
142 $\text{H}_2\text{O}/\text{Na}_2\text{O}$ ratios (Table 2). The precursor to sodium silicate solution mass ratio was kept
143 constant for all compositions. The water-to-solid ratio was calculated using the total water in
144 the mixture, including the added demineralized water, water fraction in the activation solution,
145 and total amount of solid, including the precursor and solid fraction of the activation solution.
146 The total NaOH content of the activating solution included NaOH from the sodium silicate
147 solution and added NaOH pellets. The total NaOH concentration decreased with the water-to-

148 solid ratio but remained relatively high. Based on a previous study (Cherki El Idrissi, 2019),
 149 bentonite and dispersant were added to stabilize and deflocculate the material, respectively. The
 150 activation solution was prepared first, and then the powders were added and stirred in a high-
 151 shear mixer for 5 min to ensure proper homogenization. The specimens were sealed and stored
 152 at 20 °C before characterization in a hardened state.

153

154 **Table 2 Compositions of the studied mixtures**

Mixtures		MK21	MK24	MK28	MK34
Materials	Density	Compositions (g/l)			
Metakaolin	2.63	732	671	604	518
Na-silicate	1.55	636	583	525	450
NaOH	1.46	3.3	3.0	2.7	2.3
Bentonite	2.5	9	11	13	15
Dispersant	1.4	5.5	5	4.5	4
water	1	310	367	429	511
Water to solid ratio (W/S wt.%)		0.65	0.75	0.85	1.04
Volume fractions (%)	Water	66	68	72	76
	Solid phases	34	32	28	24
Atomic ratios	Si/Al	1.83	1.83	1.83	1.83
	Na/Al	1	1	1	1
Molar ratio	H ₂ O/Na ₂ O	21	24	28	34
Total NaOH in activating solution (mol/l solution)		5.29	4.71	4.00	3.25

155

156 2.2. Testing procedures

157 2.2.1. Nuclear magnetic resonance (NMR)

158 Solid-state ^{29}Si NMR spectroscopy was performed using a Bruker Avance III 300 MHz (7 T)
159 spectrometer and a 7 mm magic angle spinning (MAS) probe, whereas ^{27}Al MAS NMR
160 spectroscopy was performed using a 500 MHz Bruker Avance III with a 2.5 mm MAS probe.
161 For ^{27}Al acquisition, the MAS speed was 30 kHz and the repetition time was set to 1 s. ^{27}Al
162 spectra were determined using a single $\pi/13$ excitation pulse for a radiofrequency field of 12
163 kHz. Chemical shifts were referenced against an $\text{Al}(\text{NO}_3)_3$ solution. For ^{29}Si acquisition, the
164 MAS speed was 5 kHz and the repetition time was set to 5 s. ^{29}Si MAS NMR spectra were
165 acquired with a single $\pi/2$ excitation of 5.5 μs . The recycle delay between scans was set to 5 s.
166 Chemical shifts were referenced against tetramethylsilane (TMS). The analysis was performed
167 on fragments obtained from crushed samples sawn from the core of hardened specimens after
168 7-, 28-, and 90-day curing in a moist room at 95% relative humidity (RH). The fragments used
169 for these tests were ground to pass through an 83 μm sieve.

170 The software Dmfit (Massiot et al., 2002) was used to decompose the ^{29}Si spectra to calculate
171 the degree of reaction. The ^{29}Si spectra were decomposed into a formed phase and a signal
172 representing remnant metakaolin. Remnant metakaolin was considered by fitting a scaled
173 component spectrum calculated from the ^{29}Si spectrum of raw metakaolin. The Gaussian lines
174 used for the decomposition of ^{29}Si spectra were defined by their intensity, peak position, and
175 full width at half height (FWHH). The overall degree of reaction RD_{ov} (**Equation 1**) could be
176 determined from the amount of formed phase in terms of Si mol%. Therefore, the reaction
177 degree was equivalent to the amount of product. In addition, the reaction degree of metakaolin
178 RD_{mk} was calculated using **Equation 2**, where $X(\text{Si})_{mk}$ and R_{mk} refer to the silicon originating
179 from metakaolin of known chemical composition and the remnant metakaolin, respectively

180 (Table 2). Only the amorphous fraction of the metakaolin was considered in the calculation.
181 The contribution of quartz at -107 ppm was not considered because of the very long relaxation
182 delays associated with the Q⁴ sites in quartz, which means that they could not be captured
183 quantitatively in the spectra. Additionally, quartz was assumed to remain unreactive during the
184 process; thus, it was not considered in the reaction progress.

$$RD_{ov}(Si) = \frac{\text{Moles of Si in product phase}}{\text{Moles of total Si in sample}} \quad \text{Equation 1}$$

$$RD_{mk} = \frac{X(Si)_{mk} - R_{mk}}{X(Si)_{mk}} \quad \text{Equation 2}$$

185 **2.2.1. Isothermal Calorimetry**

186 The short-term reactivities of the studied mixtures were characterized using an isothermal
187 calorimeter (TAM Air). The temperature was maintained at 20 °C throughout the tests. The
188 heat flow was measured, and the cumulative heat was deduced by integrating the measured
189 flux. The measurements were conducted for seven days after the end of mixing. The
190 advancement of the geopolymerization reaction was approximated by the extent of the reaction,
191 defined as the ratio of the cumulative heat at time t (Q (t)) to the ultimate heat (Q_∞). The ultimate
192 heat Q_∞ was determined by plotting the cumulative heat as a function of 1/√t (Lenormand et
193 al., 2015). A linear evolution was observed for small 1/√t values. Q_∞ was estimated as the
194 intersection of this linear function with the y-axis.

195 **2.2.2. Dynamic rheology**

196 Dynamic rheological measurements were performed using a Discovery Hybrid Rheometer from
197 TA Instruments with a vane-type configuration at a constant temperature of 20 °C. Vane
198 geometry was used to minimize the disturbance of the material during the introduction of the

199 geometry and to avoid wall slip (Saak et al., 2001). The diameters of the cup and bob were 30.36
200 and 26.198 mm respectively, providing a shear gap of 4 mm.

201 The properties of the studied mixtures in their fresh state were monitored using dynamic
202 rheology in the linear viscoelastic domain. First, the linear viscoelastic domain was determined
203 such that the measurements were nondestructive. Fresh materials were prepared and
204 immediately introduced into the bowl of the rheometer. When the material was transferred to
205 the measurement cell, residual stresses were generated and relaxed. Hence, before each test, a
206 pre-shear at 200 s^{-1} for 60 s was applied, followed by oscillation with a strain of 5% at a
207 pulsation rate of 5 rad/s (Rifaai et al., 2019) (Poulesquen et al., 2011). After the preconditioning
208 step, all experiments were performed with a strain of 0.05% (in the linear region) and pulsation
209 rate of 10 rad/s. The elastic modulus (G'), viscous modulus (G''), and loss tangent ($\tan \delta =$
210 G''/G') were analyzed during the first few hours.

211 **2.2.3. Water porosity**

212 The porosity of the material was measured at 28 and 90 days on cylindrical specimens. The
213 specimens were first saturated with water under a vacuum according to the French standard
214 procedure NF P18-459 (2010) (NF P18-459, 2010) for 4 h in air and 44 h in water. The samples
215 were then placed in an oven at $105 \text{ }^\circ\text{C}$ and weighed every day until the mass variation was lower
216 than 0.05% within 24 h to determine the dry mass. Porosity was deduced from the saturated
217 surface dry mass (SSD), dry mass (D) in air, and mass (W) in water (Equation 3).

$$\varepsilon (\%) = \frac{SSD - D}{SSD - W} * 100 \quad \text{Equation 3}$$

218 **2.2.4. Compressive strength**

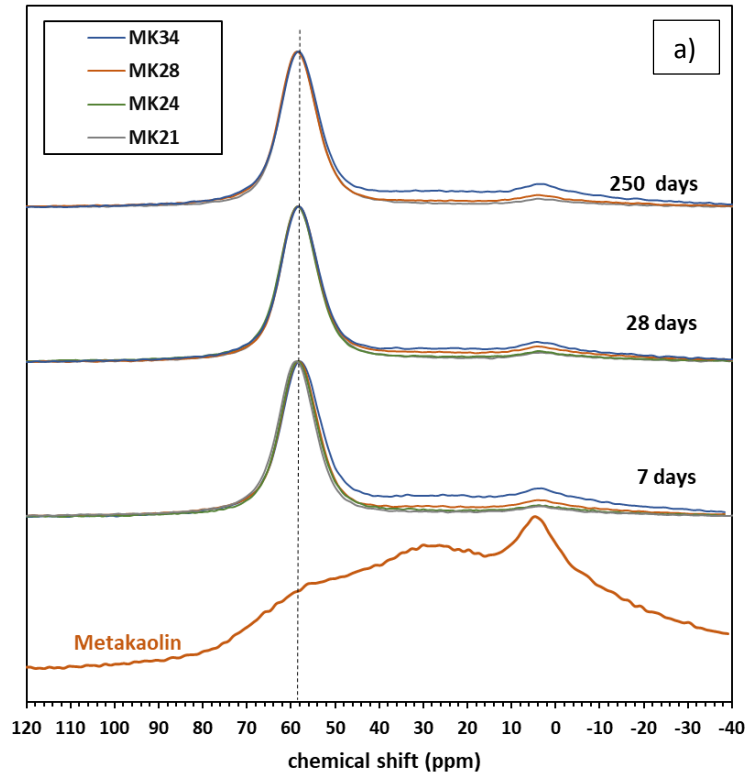
219 The test was conducted on a 100 kN press. The load rate was 1.9 kN/s until failure (NF EN
220 12390-3, 2019). Compression tests were performed on cylinders 70 mm in diameter and 140
221 mm in height at the ages of 7, 28, and 90 days. The height/diameter ratio of the tested cylinders
222 was 2, as recommended by the NF EN 12390-1 standard (NF EN 12390-1, 2012). The samples
223 were molded and cured in a room at 95% RH until compressive testing.

224 **3. Results and discussion**

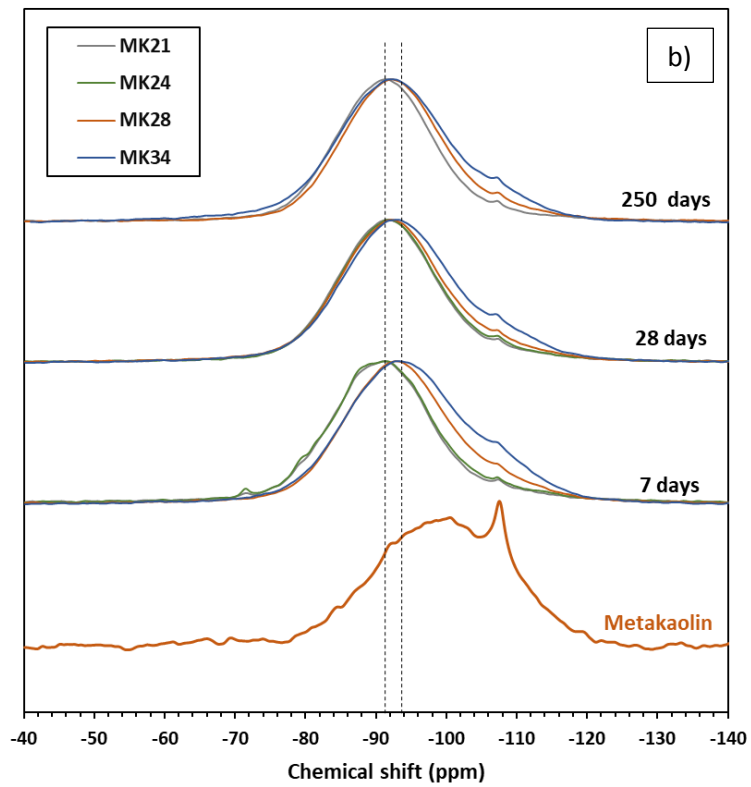
225 **3.1. Chemical characterization**

226 **3.1.1. Influence of H₂O/Na₂O on local structure**

227 ²⁷Al NMR spectra of the raw and activated metakaolin cured for 7, 28, and 250 days are
228 presented in Figure 1.a. Raw metakaolin exhibited three overlapping peaks with maxima at 55,
229 28, and 4 ppm attributed to four-, five-, and six-coordinated aluminum, respectively. The
230 activated metakaolin systems contained one predominant signal centered at 58 ppm
231 corresponding to tetrahedrally coordinated aluminum AlO₄(4Si) in the reaction products,
232 forming a three-dimensional silico-aluminate framework, which agreed with previous
233 observations of aluminosilicate-based geopolymers (Garcia-Lodeiro et al., 2015) (Davidovits
234 and Cordi, 1979). The presence of AlO₄(4Si) indicated that the concentration of charge-
235 balancing cations was sufficient to balance the negative charge of AlO₄ on the bridging oxygen
236 atoms in Si-O-Al linkages (Murdoch et al., 1985) (Perez-Cortes and Escalante-Garcia, 2020).
237 Variations in the H₂O/Na₂O ratio induced notable differences in the ²⁷Al spectra. The
238 predominant peak was observed at 58 ppm associated with Al q⁴(4Si) in the reaction products,
239 but a significant spectral intensity was also observed below 40 ppm (Al^V and Al^{VI} signals),
240 indicating that the unreacted metakaolin content increased with the H₂O/Na₂O ratio.



241



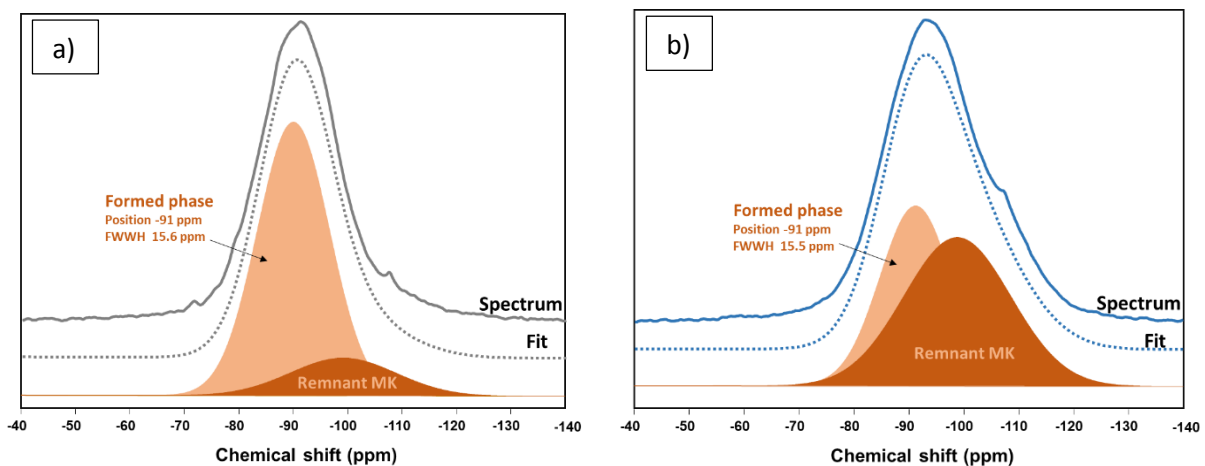
242

243

Figure 1 ^{27}Al spectra and ^{29}Si spectra of four mixtures and raw metakaolin

244 Regarding the ^{29}Si spectrum (Figure 1), the raw metakaolin spectrum presented an overall peak
 245 with a maximum at approximately -101 ppm. This broad asymmetric resonance width indicated
 246 the amorphous structure of the material. The peak detected at -107 ppm can be attributed to the
 247 quartz present in raw metakaolin (Cherki El Idrissi et al., 2018a). The activated metakaolin
 248 spectra shifted to higher frequencies, indicating structural changes in the short-ordered range.
 249 The broad width indicated the presence of Si in different environments of type $\text{Q}^4(\text{mAl})$, where
 250 m is the number of aluminum atom neighbors ($0 \leq m \leq 4$).

251 The ^{29}Si spectra were decomposed using Dmfit (Massiot et al., 2002) to form a phase and a
 252 signal representing the remnant metakaolin (Figure 2). The decomposition results are presented
 253 in Table 3.



254

255 **Figure 2** Decomposition of ^{29}Si MAS NMR spectra for a) MK21 and b) MK34 at 28 days

256 A difference was observed in the peak positions of the activated mixtures (Figure 1). For
 257 mixtures MK21 and MK24, ^{29}Si resonance appeared at -91 ppm, whereas it appeared at slightly
 258 higher frequencies (around -93 ppm) as $\text{H}_2\text{O}/\text{Na}_2\text{O}$ increased at 7 days. This variation in the
 259 peak position was only an apparent shift, as it characterized the signal induced by unreacted

260 metakaolin overlapping with that of the geopolymer. The higher the water content, the higher
 261 the unreacted metakaolin, which resulted in varying positions of the overall peak (Table 3).

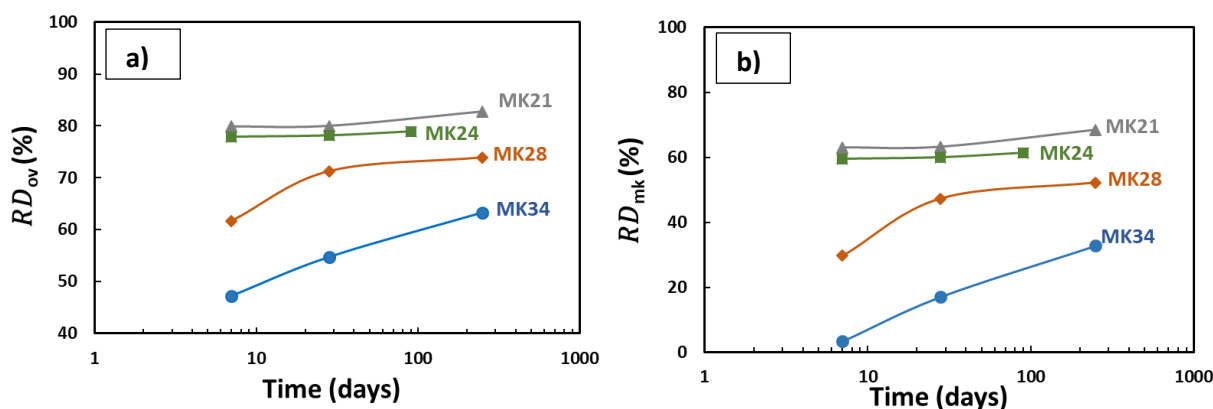
262 **Table 3 Analysis of ^{29}Si NMR spectra**

Mixtures		Remnant metakaolin	Formed phase		
		mol-%Si	Position (ppm)	FWHH	mol-%Si
MK21	7 days	20	-90.0	15.5	80
	28 days	20	-90.9	15.6	80
	250 days	17	-90.7	15.2	83
MK24	7 days	22	-91.3	15.6	78
	28 days	21	-91.3	15.1	79
	90 days	21	-90.7	15	79
MK28	7 days	38	-89.9	15.1	62
	28 days	29	-91.0	15.4	71
	250 days	26	-91.1	15.1	74
MK34	7 days	53	-91.5	15.8	47
	28 days	45	-91.1	15.5	55
	250 days	37	-91.4	16	63

263

264 The lower concentration of alkaline activator at high $\text{H}_2\text{O}/\text{Na}_2\text{O}$ content presumably resulted
 265 in a lower dissolution of silicates and aluminates from the raw material, resulting in fewer SiO_4
 266 and AlO_4 tetrahedral units to form a geopolymer gel. It was reported that increasing $\text{H}_2\text{O}/\text{Na}_2\text{O}$
 267 and $\text{Na}_2\text{O}/\text{Al}_2\text{O}_3$ tended to favor the formation of amorphous gel and various types of zeolites
 268 such as sodalite and zeolite belonging to the faujasite group, as well as zeolites X and A
 269 (Juengsuwattananon et al., 2019; Juengsuwattananon and Pimraksa, 2017). Other authors have
 270 suggested that high water content accelerates the rate of hydrolysis in systems with high Na_2O
 271 content resulting in the construction of nanocrystalline zeolite phases bound with

272 aluminosilicate gels (Zuhua et al., 2009). However, the formation of zeolitic structures or
 273 geopolymers significantly depends on the initial molar ratio, which influences the strength. The
 274 formation of zeolitic structures provides low-strength materials, whereas the formation of
 275 geopolymeric structures provides high-strength materials (Juengsuwattananon et al., 2019). A
 276 study reported that an amorphous geopolymeric phase was formed in samples with a higher
 277 initial molar ratio of $\text{SiO}_2/\text{Al}_2\text{O}_3$ (3.0–4.0) with $\text{Na}_2\text{O}/\text{Al}_2\text{O}_3$ (1.0) and $\text{H}_2\text{O}/\text{Na}_2\text{O}$ ratios in the
 278 range of 10.0–15.0; however, the study was limited to a $\text{H}_2\text{O}/\text{Na}_2\text{O}$ ratio of 20
 279 (Juengsuwattananon et al., 2019). In addition, the ^{29}Si NMR results did not exhibit any sharp
 280 peaks of different silicon environments associated with high ordering, which is typical for
 281 zeolite structures (Buchwald, 2011). Therefore, increasing the $\text{H}_2\text{O}/\text{Na}_2\text{O}$ ratio in the range of
 282 21–34 while maintaining the other molar ratios constant would not change the type of product.
 283 The overall reaction degree RD_{ov} (calculated using Equation 2) and reaction degree R_{mk}
 284 (calculated using Equation 3) are presented in **Figure 3** for all mixtures. The time evolution of
 285 the reaction degree depended on the $\text{H}_2\text{O}/\text{Na}_2\text{O}$ ratio. At $\text{H}_2\text{O}/\text{Na}_2\text{O}$ ratios of 21 and 24, the
 286 degree of reaction nearly stabilized after 7 days, whereas at higher ratios, the degree of reaction
 287 significantly increased between 7 and 250 days.

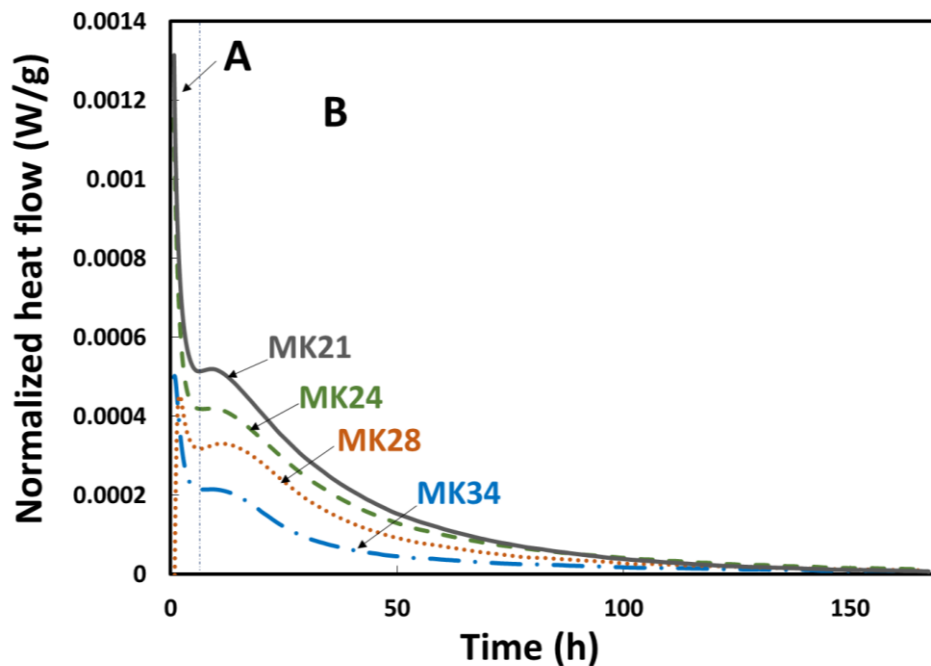


288 **Figure 3** Reaction degree as a function of time calculated from ^{29}Si NMR spectroscopy

290 From an NMR perspective, this shows that a higher amount of water delays the dissolution of
291 the precursor without blocking the reaction progress. A significant amount of the amorphous
292 fraction of metakaolin did not react even under highly alkaline conditions, as shown by R_{mk} .
293 This amount of unreacted metakaolin could be explained by the formation of a barrier layer of
294 aluminosilicate gel on the surface of metakaolin, which is likely to occur in mixtures activated
295 by a silicate solution (Chen et al., 2017).

296 3.1.2. Evolution of reaction degree

297 The heat flux released per unit weight of the material is shown in Figure 4. The first peak can
298 be attributed to the heat release caused by the wetting and dissolution of metakaolin particles,
299 which is defined as stage A.



300

301

Figure 4 Effect of water on heat flow per mass of material

302 This peak decreased with increasing H_2O/Na_2O ratios. After this stage, a second peak appeared
303 at approximately 10 and 12 h for all mixtures, with a slight shift in time as H_2O/Na_2O increased.

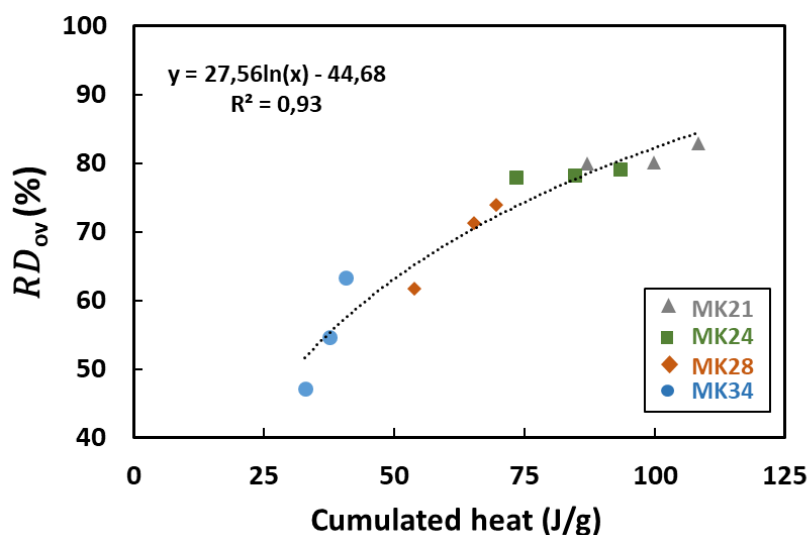
304 At a high pH, the dissolution of amorphous aluminosilicate was fast and rapidly created a
305 supersaturated aluminosilicate solution. Oligomers were then formed and polycondensated into
306 a three-dimensional system (stage B). These two stages of the geopolymerization process have
307 been distinguished for a metakaolin-based material activated with sodium silicate solution
308 (Zhang et al., 2013). After 100 h, the evolution enters a thermally steady stage, during which
309 larger networks are formed by local reorganization.

310 During the first stage (A), hydroxide ions provided by the activation solution are assumed to
311 ensure the dissolution of the aluminosilicate source and the ionization of aluminate and silicate
312 monomers (Poulesquen et al., 2011). A low-modulus $\text{SiO}_2/\text{Na}_2\text{O}$ ratio of the sodium silicate
313 activator is known to favor a high degree of geopolymerization; however, its influence on the
314 first peak is less clear (Zhang et al., 2013).

315 In this study, the Na/Al ratio and activator modulus were kept constant; moreover, the increase
316 in the $\text{H}_2\text{O}/\text{Na}_2\text{O}$ ratio might favor the dissolution of the initial solid phases owing to higher
317 concentration gradients and faster diffusion. Thus, the magnitude of the heat flux during the
318 first stage was not affected. However, the intensity of the first peak decreased significantly with
319 increasing $\text{H}_2\text{O}/\text{Na}_2\text{O}$ ratio (Figure 4). This suggests that the dissolution of the precursor and
320 the extent of reaction are influenced, on the one hand, by the available surface of metakaolin
321 exposed to alkaline solution, which in turn is related to the metakaolin content (Favier et al.,
322 2013). On the other hand, it depends on the number of free hydroxides available to dissolve the
323 metakaolin phase (Benavent et al., 2016b). The total NaOH content decreased with increasing
324 water-to-solid ratio (Table 2). Consequently, the intensity of stage A is affected by the variation
325 in the $\text{H}_2\text{O}/\text{Na}_2\text{O}$ ratio. During the polymerization stage, the rate of polycondensation decreases
326 with increasing water content. Yao et al. (Yao et al., 2009) also observed this variation in heat
327 flux with an increase in the water content of NaOH-activated metakaolin. Another study (Zuhua
328 et al., 2009) demonstrated that a higher water-to-solid ratio accelerated the dissolution and

329 hydrolysis but hindered the polycondensation. Increasing the water content while maintaining
330 other ratios constant resulted in a decrease in the exothermic peak observed in the
331 polycondensation stage with a slight shift in time.

332 The degree of reaction at 7, 28, and 250 days (determined from NMR spectra) was plotted as a
333 function of the cumulative heat obtained using isothermal calorimetry for all mixtures (Figure
334 5). The cumulative heat at 28 and 250 days was determined through extrapolation using the $1/\sqrt{t}$
335 function (Lenormand et al., 2015). The degree of reaction followed a monotonically increasing
336 trend with respect to cumulative heat. This illustrates the correlation between the analyses
337 enabled by the different characterization techniques at the chemical level. The formation of the
338 main reaction product can be directly related to the heat released and can be monitored by
339 exothermic reactions. The decrease in the heat flow observed in the calorimetry curves can be
340 attributed to the lower reaction degree of the activated metakaolin mixture.



341

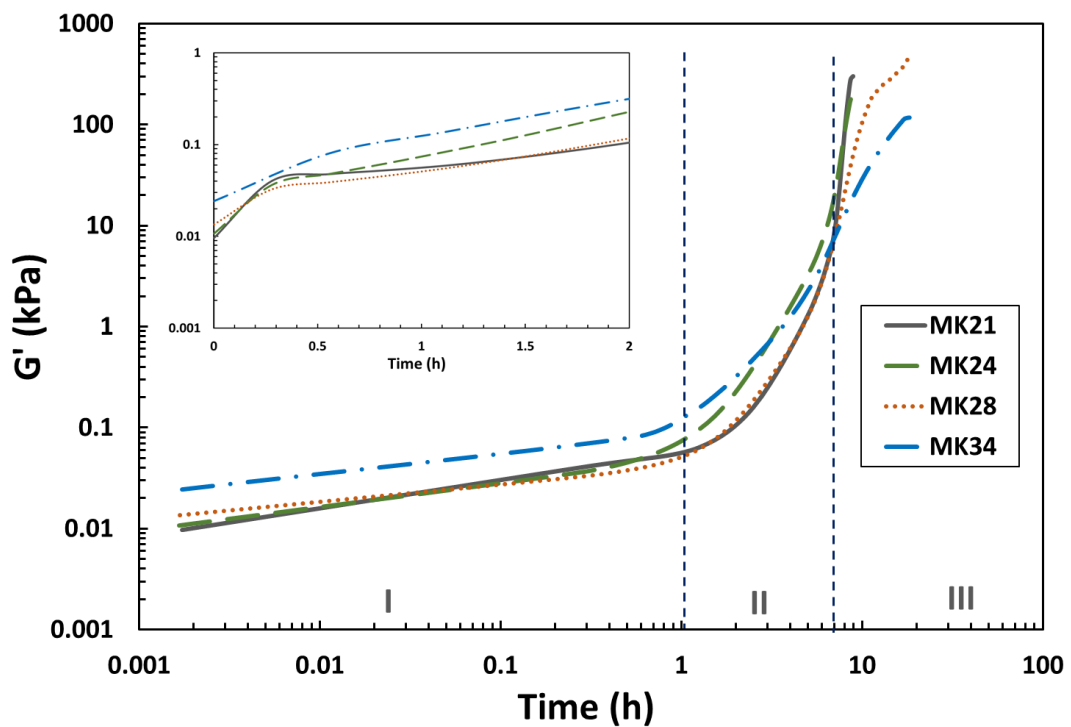
342

Figure 5 Reaction degree and cumulated heat

343 **3.2.Mechanical characterization**

344 **3.2.1. Rheological measurement**

345 The evolution of G' in the fresh state was plotted against time on a logarithmic scale for a better
346 understanding of the effect of water in the very early stages (Figure 6). G' evolved through
347 three main stages (I, II, and III in Figure 6). The first stage presents a constant growth rate, and
348 the second stage corresponds to an increasing rate of G' for all studied mixtures. The growth
349 rate during the third stage depends on the H_2O/Na_2O ratio.



350

351 *Figure 6 Evolution of elastic modulus G' as a function of time*

352 The elastic modulus of the mixture MK21 increased rapidly and reached relatively high values
353 within a short time. In contrast, the mixture MK34 exhibited a slow increase in the elastic
354 modulus and then stabilized at a low value of 22 kPa. Variations in the elastic modulus
355 suggested the formation of a more rigid network in MK21 than in MK34. At high water-to-

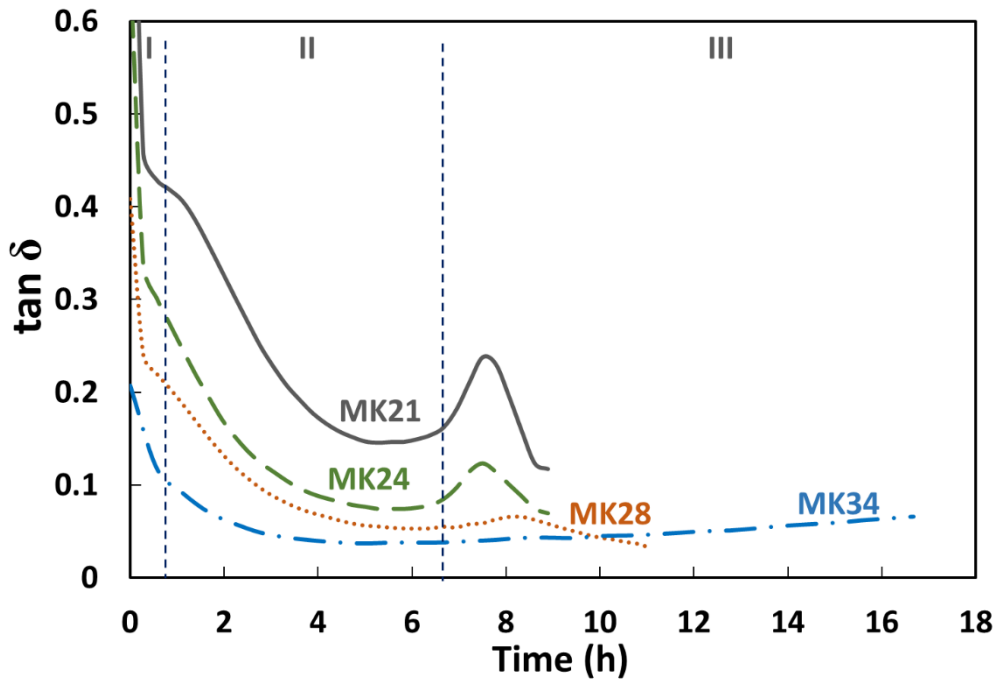
356 solid ratios, an increase in the amount of water slowed the development of mechanical
357 percolation paths. For a given reaction degree, the distance between the aluminosilicate
358 oligomers increased, and the number of mechanical percolation paths decreased. A significant
359 volume of product is required to reach the percolation threshold, resulting in a lower elastic
360 modulus (Stefan et al., 2010). Therefore, the elastic modulus remained relatively low.

361 The development of the elastic modulus as a function of H_2O/Na_2O did not follow a clear trend.
362 Different combined mechanisms may explain the variations in elastic modulus. At the
363 beginning of the first stage, the initial value of the elastic modulus is inversely correlated with
364 the H_2O/Na_2O ratio. This observation is in accordance with the attribution of the first increase
365 in the elastic modulus to the Al-rich gel formed between MK particles. Favier et al. (2013)
366 demonstrated that the colloidal interactions occurring between metakaolin particles suspended
367 in the activating solution are negligible. In addition, they observed that only low-energy
368 interactions occurred between particles as a result of the early formation of a low Si/Al
369 aluminosilicate inter-particle gel. This Al-rich gel located at the grain boundaries is responsible
370 for the initial elastic modulus. In this study, a higher H_2O/Na_2O ratio first induced faster
371 development of the elastic modulus. The concentration of the activation solution influenced the
372 kinetics of the dissolution and diffusion of aluminates $[Al(OH)_4]^-$. Thus, we can infer that a
373 higher H_2O/Na_2O ratio enhances the dissolution and diffusion of aluminates at the beginning
374 of the first stage. Consequently, despite the high water content of these mixtures, the activation
375 solution enables the dissolution and hydrolysis processes to begin. In contrast, the dissolution
376 of $[Al(OH)_4]^-$ depends on the exposed surface of metakaolin in contact with the alkaline solution
377 and the concentration of hydroxide ions, as mentioned earlier. Both the solid and liquid volume
378 fractions varied in these mixtures. Accordingly, the dissolution and diffusion of aluminate did
379 not follow a clear trend over time.

380 The mixture MK34 had the highest value of G' at a very early age. This can be attributed to the
381 easier formation of the Al-rich gel with a relatively low Si/Al ratio, as explained previously
382 (Favier et al., 2013). Another factor could be the reduced effect of the sodium silicate solution
383 (Romagnoli and Andreola, 2007). Anionic silicate oligomers present in alkaline solutions are
384 known to be highly efficient clay deflocculants, which probably increase the electrostatic
385 repulsion between particles and thus counteract attractive forces. Therefore, this effect may be
386 minimized in the mixture with a lower content of activation solution, and the amplification of
387 the elastic modulus is caused by the presence of particles, which dominate the system.

388 After a few hours, the curves intersected, and the magnitude of G' followed a different and
389 clearer trend ($G'_{21} > G'_{24} > G'_{28} > G'_{34}$). Thus, we can conclude that a new chemistry is
390 emerging, resulting in the formation of stiffer products. Favier et al. (Favier et al., 2013)
391 observed a decrease in Al concentration associated with an increasing growth rate of the elastic
392 properties. This suggests that aluminate reacts with silicate to form an aluminosilicate phase
393 with a higher Si/Al ratio.

394 The variation in $\tan \delta$ as a function of time is shown in Figure 7. First, $\tan \delta$ decreased because
395 G' varied more quickly than G'' , and it was always lower than 1 ($G' > G''$). A decrease in loss
396 factor can be attributed to the gradual gelation of the metakaolin geopolymer pastes (Rovnaník
397 et al., 2018). Subsequently, $\tan \delta$ went through a considerably constant stage. After a few hours,
398 $\tan \delta$ increased until it reached a peak value (Figure 7).



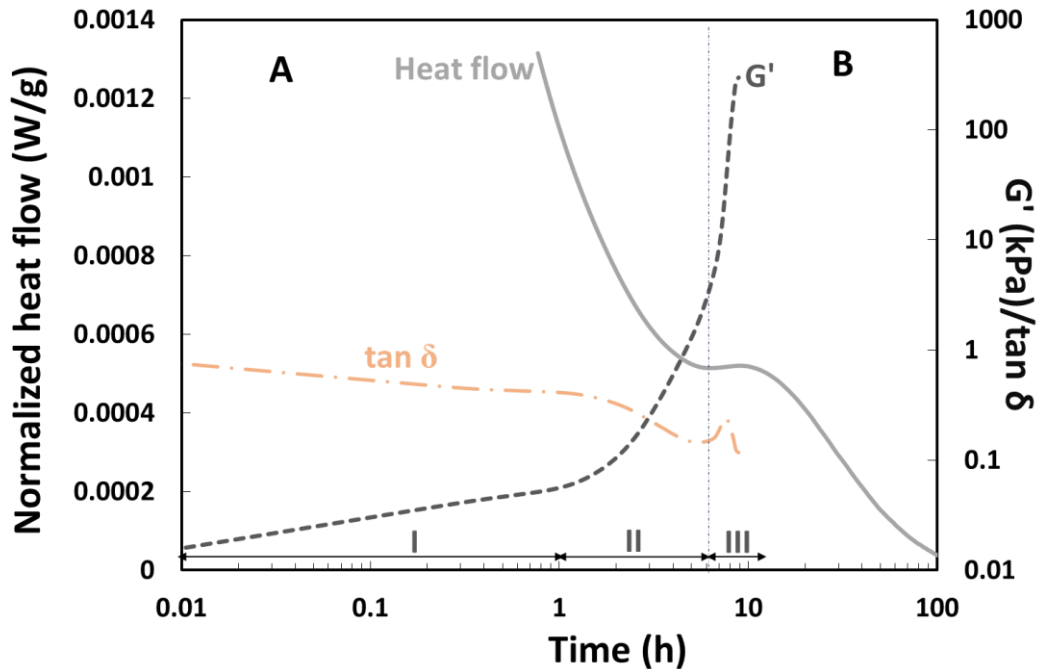
399
400 *Figure 7 Evolution of $\tan \delta$ as a function of time*

401 Several authors have mentioned that this peak presents a criterion of vitreous phase transition,
 402 which can be associated macroscopically with the gel time. Dai et al. (2020) explained this peak
 403 in the loss factor curve as the water released during the condensation reactions of the $\text{Si}(\text{OH})_4$
 404 species. After this peak, $\tan \delta$ gradually decreased, which may be due to the more indirect
 405 contact of particles, causing less loss of dissipated energy compared with more direct contact
 406 (Carreau, 2006). The rate of decrease in the loss factor after the peak was higher as the
 407 $\text{H}_2\text{O}/\text{Na}_2\text{O}$ ratio was lower. This could be attributed to a more elastic and rigid network with a
 408 low $\text{H}_2\text{O}/\text{Na}_2\text{O}$ ratio. For MK28, the time required to reach a stiffer state was longer than that
 409 for mixtures MK21 and MK24. The mixture MK34 had a steady stage in terms of the loss
 410 tangent.

411 Moreover, lower water content resulted in higher $\tan \delta$ values ($\tan \delta_{21} > \tan \delta_{24} > \tan \delta_{28}$).
 412 Normally, the $\tan \delta$ peak indicates that the dissipated energy exceeds the stored energy
 413 associated with the interactions between the constituents. Oligomer polycondensation is the

414 origin of this phenomenon. A higher polycondensation rate is expected at a lower H₂O/Na₂O
 415 ratio, which was evidenced by the higher value of the maximum tan δ in this study. Note that
 416 MK34 did not harden during this period, which was consistent with the disappearance of the
 417 maximum in the tan δ curve. This supported the assumption that the tan δ peak is associated
 418 with the beginning of the development of the final geopolymer product. This implies that tan δ
 419 can be a useful parameter for evaluating the effect of water on the magnitude of
 420 geopolymerization reactions from the early stages.

421 Dynamic rheology and isothermal calorimetry were combined to analyze the influence of the
 422 H₂O/Na₂O ratio on the behavior of fresh and hardened mixtures. G', tan δ , and heat release of
 423 MK21 are plotted in Figure 8. After a linear increase in G', the first critical point appeared, and
 424 the elastic modulus increased more rapidly but remained relatively low. The increase in G' may
 425 be due to further dissolution of metakaolin particles and the formation of large oligomers.



426

427

Figure 8 Correlation between G', tan δ , and heat flow for MK21

428 At the beginning of stage B, a second critical point occurred, and the G' growth rate further
429 increased. During this stage, G' reached high values after a short time. The rapid increase in the
430 elastic modulus can be associated with the formation of large oligomers or the initiation of
431 polycondensation into a three-dimensional network, often called a geopolymer structure. These
432 critical points can be more easily distinguished for MK21 and MK24 mixtures than for MK28
433 and MK34.

434 The second critical point of the different mixtures appeared at approximately the same time,
435 but with different rate variations (Figure 6). This result suggested that all mixtures reached
436 supersaturation simultaneously. This corresponded to a critical Si/Al ratio, which was
437 consistent with the composition of the studied mixtures, as the Si/Al and Na/Al ratios were kept
438 constant. The main difference between these mixtures was the water content. However, it has
439 been demonstrated that water does not affect silicate species' condensation in alkaline silicate
440 solutions (Bourlon, 2010). This agrees with the results of NMR spectroscopy (see Section
441 3.1.1), which indicated that the local structure of the reaction products was not affected by the
442 initial water content.

443 Consequently, the consistency between the evolution of the reaction rate and the evolution of
444 the elastic modulus G' of the materials can be highlighted. An origin at the physicochemical
445 level can be assumed. Studies have shown that an increase in the consumption of metakaolin is
446 accompanied by an increase in the shear modulus of geopolymers. Similarly, the stabilization
447 of the consumption rate of metakaolin corresponds to the setting of the geopolymer (Bourlon,
448 2010).

449 **3.2.2. Correlations between mechanical properties and chemical reaction degree**

450 The compressive strength was measured at 7, 28, and 90 d for all mixtures except MK34. Its
451 compressive strength was lower than 25 kPa after 90 days, which corresponded to the minimum
452 compressive strength measurable by the machine on cylindrical specimens.

453 Table 4 lists the heat released, compressive strength, and water porosity at different ages. The
454 cumulative heat at 7 days was directly deduced from the experimental data of isothermal
455 calorimetry (Figure 4), and the cumulative heat at 28 days was determined by extrapolation
456 using the $1/\sqrt{t}$ function (Lenormand et al., 2015). The compressive strengths of all mixtures
457 primarily developed within the first 7 days. From the values at 7 and 28 days, the strength
458 development was not proportional to the cumulative released heat. Mixtures MK21 and MK24
459 had nearly the same cumulative heat at 7 and 28 days, but they exhibited significantly different
460 values of compressive strength. Thus, the data from calorimetry were not sufficient to explain
461 the development of strength, particularly the decrease in strength owing to the increase in the
462 H_2O/Na_2O ratio from 21 to 28. This confirms that strength development also depends on the
463 physical and microstructural parameters of the material. Thus, the water porosities at 28 and 90
464 days were also determined.

465 The porosity of the hardened material was proportional to the initial water content (Table 4).
466 This means that the pores replaced the main part of the initial water volume in the hardened
467 material, which was consistent with a previous study (Pouhet et al., 2019). Studies show that
468 the amount of water in the initial geopolymer system is the dominant factor affecting the density
469 and open porosity after extended aging (Benavent et al., 2016a; Lizcano et al., 2012). This
470 influence of porosity on strength is a priori similar to the behavior of ceramics, as the strength
471 exponentially decreases with porosity (Kingery et al., 1976) (Biswas, 1976). The literature
472 indicates that maintaining an H_2O/Na_2O ratio between 10 and 20 is necessary to achieve

473 significant strength for a structural geopolymer (Cui, 2019). From the experimental results, a
 474 higher value of this ratio can enable the performance required for different applications to be
 475 attained, where high strength is not the main interest, provided that the materials exhibit the
 476 expected values of elastic modulus, water permeability, fire resistance, etc. A decrease in the
 477 strength and geopolymer content (Figure 9) was observed at approximately $H_2O/Na_2O = 30$.

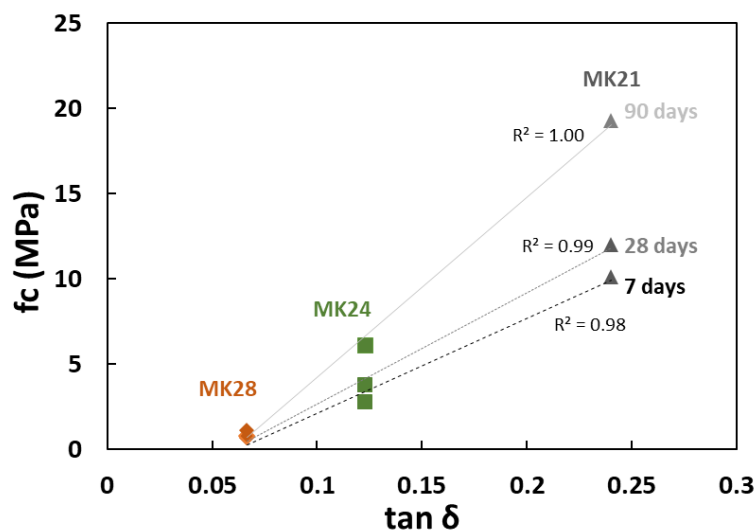
478 A significant increase in the compressive strength occurred between 28 and 90 days, as shown
 479 in Table 4. However, the reaction degree of MK21, MK24, and MK28 mixtures did not
 480 significantly increase during this period (Figure 3). The porosity slightly decreased between 28
 481 and 90 days, which may partially explain the increase in the compressive strength. The
 482 refinement of the porosity of an activated metakaolin over time was attributed to the
 483 densification of the solid network and partial closure of the porosity at the nanometer scale
 484 (Steins et al., 2014). Moreover, a dissolution–precipitation mechanism occurring at the pore
 485 wall interface was observed, which could explain the slight decrease in the pore volume
 486 (Benavent et al., 2016a).

487 **Table 4 Released heat, compressive strength, and porosity after different ages**

Age (days)	Initial water (% vol)	Porosity (% vol.)		Released heat (J/g)		Compressive strength (MPa)		
		28	90	7	28	7	28	90
MK21	66	60.3	59.7	87.1	100	10.1	12.0	19.3
MK24	68	64.0	62.9	72.1	84.9	2.7	3.8	6.0
MK28	72	68.8	68.2	59.0	65.5	0.7	0.8	1.1
MK34	76	-	-	32.9	37.6	< 0.025	< 0.025	< 0.025

488

489 The compressive strength was plotted as a function of $\tan \delta$ obtained from rheological
 490 measurements (Figure 9). The maximum $\tan \delta$ obtained by rheological testing is linearly
 491 correlated with the compressive strength at 7, 28, and 90 days. This correlation between the
 492 mechanical properties at an early age and long-term results from multiple parameters, such as
 493 the reaction degree, microstructure parameters, and their time evolution. Steins et al. (2012)
 494 mentioned that the variation in the value of $\tan \delta$ is difficult to explain. As a word of caution
 495 before generalizing this correlation, note that it strongly depends on the material composition
 496 and examined objectives. In addition, MK34 did not develop significant mechanical strength
 497 even after 90 days, which was consistent with the disappearance of the maximum $\tan \delta$ for this
 498 mixture.



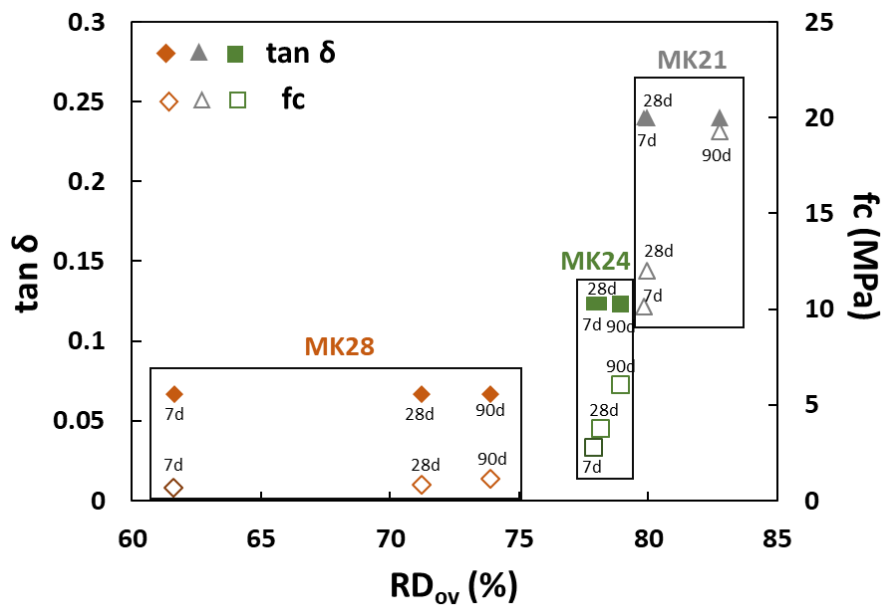
499

500 **Figure 9 Compressive strength as a function of the maximum of $\tan \delta$**

501 Finally, the compressive strength and maximum $\tan \delta$ are plotted as a function of the degree of
 502 reaction in Figure 10. A decrease in compressive strength was observed with an increase in the
 503 H_2O/Na_2O ratio. It has been reported that the compressive strength is linearly correlated with
 504 the reaction degree (Chen et al., 2020). However, in this study, the compressive strength was
 505 not correlated with the degree of reaction. MK21 and MK24 exhibited similar reaction degrees
 506 but developed different compressive strengths. Conversely, the significant increase in the

507 reaction degrees from MK28 to MK24 resulted in limited strength development. Both strength
 508 and $\tan \delta$ can be considered mechanical parameters. For instance, $\tan \delta$ was deduced from the
 509 G' values, which also sharply decreased with the H_2O/Na_2O ratio (Figure 6). The strength and
 510 $\tan \delta$ depend on the chemical reactivity of the binder, but not directly, as they are also influenced
 511 by the initial porosity and packing density of the mixture, the development of percolation paths,
 512 the intrinsic mechanical properties of each phase, and their complex interactions that influence
 513 the time evolution of the microstructure.

514 Based on this, $\tan \delta$ appears to be a useful parameter to anticipate the influence of the H_2O/Na_2O
 515 ratio on strength from short-term rheological measurements, and the correlation with strength
 516 enables us to understand its evolution.



517

518 *Figure 10 Compressive strength and $\tan \delta$ versus the degree of reaction*

519

520 4. Conclusions

521 Metakaolin-based geopolymers were characterized using advanced experimental and analytical
522 techniques to monitor the reaction advancement and development of mechanical properties
523 from the fresh to the hardened state. The mixtures were designed by keeping the molar ratios
524 constant, only the H₂O/Na₂O ratio varied from 21 to 34. The following conclusions were drawn:

- 525 • The analysis of the phase composition suggested that water did not affect the structure
526 of the geopolymer-type phase. A higher H₂O/Na₂O ratio resulted in a higher content of
527 unreacted metakaolin and a lower product fraction, as shown by the NMR results.
- 528 • The combination of isothermal calorimetry and dynamic rheology allows to distinguish
529 the different stages of the structuration of fresh and hardening materials.
- 530 • The maximum loss tangent $\tan \delta$ appeared to be a reliable indicator for estimating the
531 sensitivity of the strength of the studied mixtures to the initial water content.
- 532 • At the chemical mechanism level, a correlation between the cumulated released heat
533 obtained by isothermal calorimetry and the degree of reaction deduced from the
534 decomposition of NMR spectra was revealed.
- 535 • The maximum $\tan \delta$ obtained using the rheological test was linearly correlated with the
536 compressive strength. The degree of reaction and mechanical properties were poorly
537 correlated at the studied scales of time and space. The decrease in compressive strength
538 with H₂O/Na₂O ratio was explained by the influence of water on the reactivity of the
539 precursor and the higher porosity of the material, as the water was not chemically bound.

540 References

- 541 Aboulayt, A., Jaafri, R., Samouh, H., Cherki El Idrissi, A., Roziere, E., Moussa, R., Loukili,
542 A., 2018. Stability of a new geopolymer grout: Rheological and mechanical
543 performances of metakaolin-fly ash binary mixtures. *Construction and Building*
544 *Materials* 181, 420–436. <https://doi.org/10.1016/j.conbuildmat.2018.06.025>
- 545 Aboulayt, A., Souayfan, F., Roziere, E., Jaafri, R., Cherki El Idrissi, A., Moussa, R., Justino,
546 C., Loukili, A., 2020. Alkali-activated grouts based on slag-fly ash mixtures: From

547 early-age characterization to long-term phase composition. *Construction and Building*
548 *Materials* 260, 120510. <https://doi.org/10.1016/j.conbuildmat.2020.120510>

549 Benavent, V., Frizon, F., Poulesquen, A., 2016a. Effect of composition and aging on the porous
550 structure of metakaolin-based geopolymers. *J Appl Crystallogr* 49, 2116–2128.
551 <https://doi.org/10.1107/S1600576716014618>

552 Benavent, V., Steins, P., Sobrados, I., Sanz, J., Lambertin, D., Frizon, F., Rossignol, S.,
553 Poulesquen, A., 2016b. Impact of aluminum on the structure of geopolymers from the
554 early stages to consolidated material. *Cement and Concrete Research* 90, 27–35.
555 <https://doi.org/10.1016/j.cemconres.2016.09.009>

556 Biswas, D.R., 1976. Influence of porosity on the mechanical properties of lead zirconate--
557 titanate ceramics (No. LBL-5479, 7110774). <https://doi.org/10.2172/7110774>

558 Bourlon, A., 2010. Physico-chimie et rhéologie de géopolymères frais pour la cimentation des
559 puits pétroliers, in french (PhD thesis). Université Paris VI.

560 Bruno, S., Claude, P., Laurent, B., Philippe, L., 2018. Amélioration et renforcement des sols -
561 AMSOL - Tome 2, in french, LE MONITEUR. ed.

562 Buchwald, A., 2011. Condensation of aluminosilicate gels—model system for geopolymer
563 binders. *Journal of Non-Crystalline Solids* 7.
564 <https://doi.org/10.1016/j.jnoncrysol.2010.12.036>

565 Carreau, P.J., 2006. Philippe Coussot: Rheometry of Pastes, Suspensions and Granular
566 Materials. Applications in Industry and Environment: JohnWiley and Sons, Inc.,
567 Hoboken, New Jersey. ISBN 0-471-65369-1, 291 pages, US \$89.95. *Rheol Acta* 46,
568 317–318. <https://doi.org/10.1007/s00397-006-0118-y>

569 Chen, X., Kim, E., Suraneni, P., Struble, L., 2020. Quantitative Correlation between the Degree
570 of Reaction and Compressive Strength of Metakaolin-Based Geopolymers. *Materials*
571 13, 5784. <https://doi.org/10.3390/ma13245784>

572 Chen, X., Sutrisno, A., Zhu, L., Struble, L.J., 2017. Setting and nanostructural evolution of
573 metakaolin geopolymer. *J Am Ceram Soc* 100, 2285–2295.
574 <https://doi.org/10.1111/jace.14641>

575 Cherki El Idrissi, A., 2019. The development of a global mix design and analysis approach for
576 alkali activated soil reinforcement grouts. *European Journal of Environmental and Civil*
577 *Engineering* 23, 645–656. <https://doi.org/10.1080/19648189.2018.1519461>

578 Cherki El Idrissi, A., Paris, M., Rozière, E., Deneele, D., Darson, S., Loukili, A., 2018a. Alkali-
579 activated grouts with incorporated fly ash: From NMR analysis to mechanical
580 properties. *Materials Today Communications* 14, 225–232.
581 <https://doi.org/10.1016/j.mtcomm.2018.01.012>

582 Cherki El Idrissi, A., Roziere, E., Loukili, A., Darson, S., 2018b. Design of geopolymer grouts:
583 the effects of water content and mineral precursor. *European Journal of Environmental*
584 *and Civil Engineering* 22, 628–649. <https://doi.org/10.1080/19648189.2016.1214183>

585 Clausi, M., Tarantino, S.C., Magnani, L.L., Riccardi, M.P., Tedeschi, C., Zema, M., 2016.
586 Metakaolin as a precursor of materials for applications in Cultural Heritage:
587 Geopolymer-based mortars with ornamental stone aggregates. *Applied Clay Science*
588 132–133, 589–599. <https://doi.org/10.1016/j.clay.2016.08.009>

589 Costa, L.M., Almeida, N.G.S., Houmard, M., Cetlin, P.R., Silva, G.J.B., Aguilar, M.T.P., 2021.
590 Influence of the addition of amorphous and crystalline silica on the structural properties
591 of metakaolin-based geopolymers. *Applied Clay Science* 215, 106312.
592 <https://doi.org/10.1016/j.clay.2021.106312>

593 Cui, Y., 2019. Effects of the n(H₂O_ Na₂Oeq) ratio on the geopolymerization process and
594 microstructures of fly ash-based geopolymers. *Journal of Non-Crystalline Solids* 10.
595 <https://doi.org/10.1016/j.jnoncrysol.2018.12.033>

596 Dai, X., Aydin, S., Yardimci, M.Y., Lesage, K., de Schutter, G., 2020. Influence of water to
597 binder ratio on the rheology and structural Build-up of Alkali-Activated Slag/Fly ash
598 mixtures. *Construction and Building Materials* 264, 120253.
599 <https://doi.org/10.1016/j.conbuildmat.2020.120253>

600 Davidovits, J., Cordi, S.A., 1979. Synthesis of New High-Temperature Geo-Polymers for
601 Reinforced Plastics/Composites. *Annu. Pac. Tech. Conf. Tech. Disp* 4 151–154.

602 Duxson, P., Fernández-Jiménez, A., Provis, J.L., Lukey, G.C., Palomo, A., van Deventer, J.S.J.,
603 2007. Geopolymer technology: the current state of the art. *J Mater Sci* 42, 2917–2933.
604 <https://doi.org/10.1007/s10853-006-0637-z>

605 Etemadi, H., Afsharkia, S., Zinatloo- Ajabshir, S., Shokri, E., 2021. Effect of alumina
606 nanoparticles on the antifouling properties of polycarbonate- polyurethane blend
607 ultrafiltration membrane for water treatment. *Polym Eng Sci* 61, 2364–2375.
608 <https://doi.org/10.1002/pen.25764>

609 Favier, A., Habert, G., d’Espinoze de Lacaillerie, J.B., Roussel, N., 2013. Mechanical properties
610 and compositional heterogeneities of fresh geopolymer pastes. *Cement and Concrete*
611 *Research* 48, 9–16. <https://doi.org/10.1016/j.cemconres.2013.02.001>

612 Favier, Aurélie, Hot, J., Habert, G., Roussel, N., 2013. RHEOLOGY OF GEOPOLYMER:
613 COMPARATIVE STUDY BETWEEN PORTLAND CEMENT AND METAKAOLIN
614 BASED GEOPOLYMER 8.

615 Gadkar, A., Subramaniam, K.V.L., 2019. An evaluation of yield and Maxwell fluid behaviors
616 of fly ash suspensions in alkali-silicate solutions. *Mater Struct* 52, 117.
617 <https://doi.org/10.1617/s11527-019-1429-7>

618 Garcia-Lodeiro, I., Palomo, A., Fernández-Jiménez, A., 2015. An overview of the chemistry of
619 alkali-activated cement-based binders, in: *Handbook of Alkali-Activated Cements,*
620 *Mortars and Concretes.* Elsevier, pp. 19–47.
621 <https://doi.org/10.1533/9781782422884.1.19>

622 Güllü, H., Al Nuaimi, M.M.D., Aytek, A., 2020. Rheological and strength performances of
623 cold-bonded geopolymer made from limestone dust and bottom ash for grouting and
624 deep mixing. *Bull Eng Geol Environ.* <https://doi.org/10.1007/s10064-020-01998-2>

625 Güllü, H., Cevik, A., Al-Ezzi, K.M.A., Gülsan, M.E., 2019. On the rheology of using
626 geopolymer for grouting: A comparative study with cement-based grout included fly
627 ash and cold bonded fly ash. *Construction and Building Materials* 196, 594–610.
628 <https://doi.org/10.1016/j.conbuildmat.2018.11.140>

629 Hassan, A., Arif, M., Shariq, M., 2019. Use of geopolymer concrete for a cleaner and
630 sustainable environment – A review of mechanical properties and microstructure.
631 *Journal of Cleaner Production* 223, 704–728.
632 <https://doi.org/10.1016/j.jclepro.2019.03.051>

633 Hwalla, J., Saba, M., Assaad, J.J., 2020. Suitability of metakaolin-based geopolymers for
634 underwater applications. *Mater Struct* 53, 119. [https://doi.org/10.1617/s11527-020-](https://doi.org/10.1617/s11527-020-01546-0)
635 [01546-0](https://doi.org/10.1617/s11527-020-01546-0)

636 Juengsuwattananon, K., Pimraksa, K., 2017. Variable factors controlling amorphous-zeolite
637 phase transformation in metakaolin based geopolymer. *Acta Metall Slovaca* 23, 378–
638 386. <https://doi.org/10.12776/ams.v23i4.1001>

639 Juengsuwattananon, K., Winnefeld, F., Chindaprasirt, P., Pimraksa, K., 2019. Correlation
640 between initial SiO₂/Al₂O₃, Na₂O/Al₂O₃, Na₂O/SiO₂ and H₂O/Na₂O ratios on phase
641 and microstructure of reaction products of metakaolin-rice husk ash geopolymer.
642 *Construction and Building Materials* 226, 406–417.
643 <https://doi.org/10.1016/j.conbuildmat.2019.07.146>

644 Kingery, W.D., Bowen, H.K., Uhlmann, D.R., 1976. *Introduction to ceramics*, Wilet. ed. New
645 York.

646 Lenormand, T., Rozière, E., Loukili, A., Staquet, S., 2015. Incorporation of treated municipal
647 solid waste incineration electrostatic precipitator fly ash as partial replacement of
648 Portland cement: Effect on early age behaviour and mechanical properties. *Construction*
649 and *Building Materials* 96, 256–269.
650 <https://doi.org/10.1016/j.conbuildmat.2015.07.171>

651 Leonelli, C., Romagnoli, M., 2015. Rheology parameters of alkali-activated geopolymeric
652 concrete binders, in: *Handbook of Alkali-Activated Cements, Mortars and Concretes*.
653 Elsevier, pp. 133–169. <https://doi.org/10.1533/9781782422884.2.133>

654 Liu, X., Jiang, J., Zhang, H., Li, M., Wu, Y., Guo, L., Wang, W., Duan, P., Zhang, W., Zhang,
655 Z., 2020. Thermal stability and microstructure of metakaolin-based geopolymer blended
656 with rice husk ash. *Applied Clay Science* 196, 105769.
657 <https://doi.org/10.1016/j.clay.2020.105769>

658 Lizcano, M., Gonzalez, A., Basu, S., Lozano, K., Radovic, M., 2012. Effects of Water Content
659 and Chemical Composition on Structural Properties of Alkaline Activated Metakaolin-
660 Based Geopolymers. *J. Am. Ceram. Soc.* 95, 2169–2177.
661 <https://doi.org/10.1111/j.1551-2916.2012.05184.x>

662 Mahdavi, K., Zinatloo-Ajabshir, S., Yousif, Q.A., Salavati-Niasari, M., 2022. Enhanced
663 photocatalytic degradation of toxic contaminants using Dy₂O₃-SiO₂ ceramic
664 nanostructured materials fabricated by a new, simple and rapid sonochemical approach.
665 *Ultrasonics Sonochemistry* 82, 105892. <https://doi.org/10.1016/j.ultsonch.2021.105892>

666 Massiot, D., Fayon, F., Capron, M., King, I., Le Calvé, S., Alonso, B., Durand, J.-O., Bujoli,
667 B., Gan, Z., Hoatson, G., 2002. Modelling one- and two-dimensional solid-state NMR
668 spectra: Modelling 1D and 2D solid-state NMR spectra. *Magn. Reson. Chem.* 40, 70–
669 76. <https://doi.org/10.1002/mrc.984>

670 Murdoch, J.B., Stebbins, J.F., Carmichael, I.S.E., 1985. High-resolution ²⁹Si NMR study of
671 silicate and aluminosilicate glasses: the effect of network-modifying cations. *American*
672 *Mineralogist* 70, 332–343.

673 NF EN 12390-1, 2012. Testing hardened concrete - Part 1 : shape, dimensions and other
674 requirements for specimens and moulds. AFNOR.

675 NF EN 12390-3, 2019. Testing hardened concrete - Part 3 : compressive strength of test
676 specimens. AFNOR.

677 NF P18-459, 2010. Concrete - Testing hardened concrete - Testing porosity and density.
678 AFNOR.

679 Panias, D., Giannopoulou, I.P., Perraki, T., 2007. Effect of synthesis parameters on the
680 mechanical properties of fly ash-based geopolymers. *Colloids and Surfaces A:*
681 *Physicochemical and Engineering Aspects* 301, 246–254.
682 <https://doi.org/10.1016/j.colsurfa.2006.12.064>

683 Perez-Cortes, P., Escalante-Garcia, J.I., 2020. Gel composition and molecular structure of
684 alkali-activated metakaolin-limestone cements. *Cement and Concrete Research* 13.
685 <https://doi.org/10.1016/j.cemconres.2020.106211>

686 Pouhet, R., Cyr, M., Bucher, R., 2019. Influence of the initial water content in flash calcined
687 metakaolin-based geopolymer. *Construction and Building Materials* 201, 421–429.
688 <https://doi.org/10.1016/j.conbuildmat.2018.12.201>

689 Poulesquen, A., Frizon, F., Lambertin, D., 2011. Rheological behavior of alkali-activated
690 metakaolin during geopolymerization. *Journal of Non-Crystalline Solids* 357, 3565–
691 3571. <https://doi.org/10.1016/j.jnoncrysol.2011.07.013>

692 Provis, J., 2013. Alkali activated materials: state-of-the-art report, RILEM TC 224-AAM,
693 Springer Science&Business Media. ed. Springer, New York.

694 Provis, J.L., 2014. Geopolymers and other alkali activated materials: why, how, and what?
695 *Mater Struct* 15. <https://doi.org/10.1617/s11527-013-0211-5>

696 Provis, J.L., Yong, C.Z., Duxson, P., van Deventer, J.S.J., 2009. Correlating mechanical and
697 thermal properties of sodium silicate-fly ash geopolymers. *Colloids Surf. A: Physicochem. Eng. Asp* 57–63.
698
699 Rifaai, Y., Yahia, A., Mostafa, A., Aggoun, S., Kadri, E.-H., 2019. Rheology of fly ash-based
700 geopolymer: Effect of NaOH concentration. *Construction and Building Materials* 223,
701 583–594. <https://doi.org/10.1016/j.conbuildmat.2019.07.028>
702 Romagnoli, M., Andreola, F., 2007. Mixture of deflocculants: A systematic approach. *Journal*
703 *of the European Ceramic Society* 27, 1871–1874.
704 <https://doi.org/10.1016/j.jeurceramsoc.2006.05.065>
705 Rovnaník, P., Rovnaníková, P., Vyšvařil, M., Grzeszczyk, S., Janowska-Renkas, E., 2018.
706 Rheological properties and microstructure of binary waste red brick powder/metakaolin
707 geopolymer. *Construction and Building Materials* 188, 924–933.
708 <https://doi.org/10.1016/j.conbuildmat.2018.08.150>
709 Saak, A.W., Jennings, H.M., Shah, S.P., 2001. The influence of wall slip on yield stress and
710 viscoelastic measurements of cement paste. *Cement and Concrete Research* 31, 205–
711 212. [https://doi.org/10.1016/S0008-8846\(00\)00440-3](https://doi.org/10.1016/S0008-8846(00)00440-3)
712 San Nicolas, R., Cyr, M., Escadeillas, G., 2013. Characteristics and applications of flash
713 metakaolins. *Applied Clay Science* 83–84, 253–262.
714 <https://doi.org/10.1016/j.clay.2013.08.036>
715 Sathonsaowaphak, A., Chindapasirt, P., Pimraksa, K., 2009. Workability and strength of
716 lignite bottom ash geopolymer mortar. *Journal of Hazardous Materials* 168, 44–50.
717 <https://doi.org/10.1016/j.jhazmat.2009.01.120>
718 Scrivener, K., Martirena, F., Bishnoi, S., Maity, S., 2018. Calcined clay limestone cements
719 (LC3). *Cement and Concrete Research* 114, 49–56.
720 <https://doi.org/10.1016/j.cemconres.2017.08.017>
721 Souayfan, F., Rozière, E., Paris, M., Deneele, D., Loukili, A., Justino, C., 2022. ²⁹Si and ²⁷Al
722 MAS NMR spectroscopic studies of activated metakaolin-slag mixtures. *Construction*
723 *and Building Materials* 322, 126415.
724 <https://doi.org/10.1016/j.conbuildmat.2022.126415>
725 Stefan, L., Benboudjema, F., Torrenti, J.-Michel., Bissonnette, B., 2010. Prediction of elastic
726 properties of cement pastes at early ages. *Computational Materials Science* 47, 775–
727 784. <https://doi.org/10.1016/j.commatsci.2009.11.003>
728 Steins, P., Poulesquen, A., Diat, O., Frizon, F., 2012. Structural Evolution during
729 Geopolymerization from an Early Age to Consolidated Material. *Langmuir* 28, 8502–
730 8510. <https://doi.org/10.1021/la300868v>
731 Steins, P., Poulesquen, A., Frizon, F., Diat, O., Jestin, J., Causse, J., Lambertin, D., Rossignol,
732 S., 2014. Effect of aging and alkali activator on the porous structure of a geopolymer. *J*
733 *Appl Crystallogr* 47, 316–324. <https://doi.org/10.1107/S160057671303197X>
734 Turner, L.K., Collins, F.G., 2013. Carbon dioxide equivalent (CO₂-e) emissions: A comparison
735 between geopolymer and OPC cement concrete. *Construction and Building Materials*
736 43, 125–130. <https://doi.org/10.1016/j.conbuildmat.2013.01.023>
737 Weng, L., Sagoe-Crentsil, K., 2007. Dissolution processes, hydrolysis and condensation
738 reactions during geopolymer synthesis: Part I—Low Si/Al ratio systems. *J Mater Sci*
739 42, 2997–3006. <https://doi.org/10.1007/s10853-006-0820-2>
740 Wu, Y., Lu, B., Yi, Z., Du, F., Zhang, Y., 2019. The Properties and Latest Application of
741 Geopolymers. *IOP Conf. Ser.: Mater. Sci. Eng.* 472, 012029.
742 <https://doi.org/10.1088/1757-899X/472/1/012029>
743 Yaghoubi, M., Arulrajah, A., Disfani, M.M., Horpibulsuk, S., Darmawan, S., Wang, J., 2019.
744 Impact of field conditions on the strength development of a geopolymer stabilized

- 745 marine clay. *Applied Clay Science* 167, 33–42.
746 <https://doi.org/10.1016/j.clay.2018.10.005>
- 747 Yahya, Z., Abdullah, M., Hussin, K., Ismail, K., Razak, R., Sandu, A., 2015. Effect of Solids-
748 To-Liquids, Na₂SiO₃-To-NaOH and Curing Temperature on the Palm Oil Boiler Ash
749 (Si + Ca) Geopolymerisation System. *Materials* 8, 2227–2242.
750 <https://doi.org/10.3390/ma8052227>
- 751 Yang, J., Xu, L., Wu, H., Jin, J., Liu, L., 2022. Microstructure and mechanical properties of
752 metakaolin-based geopolymer composites containing high volume of spodumene
753 tailings. *Applied Clay Science* 218, 106412. <https://doi.org/10.1016/j.clay.2022.106412>
- 754 Yao, X., Zhang, Z., Zhu, H., Chen, Y., 2009. Geopolymerization process of alkali-
755 metakaolinite characterized by isothermal calorimetry. *Thermochimica Acta* 493, 49–
756 54. <https://doi.org/10.1016/j.tca.2009.04.002>
- 757 Zhang, B., Guo, H., Yuan, P., Li, Y., Wang, Q., Deng, L., Liu, D., 2020. Geopolymerization of
758 halloysite via alkali-activation: Dependence of microstructures on precalcination.
759 *Applied Clay Science* 185, 105375. <https://doi.org/10.1016/j.clay.2019.105375>
- 760 Zhang, B., Yuan, P., Guo, H., Deng, L., Li, Y., Li, L., Wang, Q., Liu, D., 2021. Effect of curing
761 conditions on the microstructure and mechanical performance of geopolymers derived
762 from nanosized tubular halloysite. *Construction and Building Materials* 268, 121186.
763 <https://doi.org/10.1016/j.conbuildmat.2020.121186>
- 764 Zhang, M., Zhao, M., Zhang, G., Nowak, P., Coen, A., Tao, M., 2015. Calcium-free
765 geopolymer as a stabilizer for sulfate-rich soils. *Applied Clay Science* 108, 199–207.
766 <https://doi.org/10.1016/j.clay.2015.02.029>
- 767 Zhang, Z., Provis, J.L., Wang, H., Bullen, F., Reid, A., 2013. Quantitative kinetic and structural
768 analysis of geopolymers. Part 2. Thermodynamics of sodium silicate activation of
769 metakaolin. *Thermochimica Acta* 565, 163–171.
770 <https://doi.org/10.1016/j.tca.2013.01.040>
- 771 Zinatloo-Ajabshir, S., Baladi, M., Salavati-Niasari, M., 2021. Sono-synthesis of MnWO₄
772 ceramic nanomaterials as highly efficient photocatalysts for the decomposition of toxic
773 pollutants. *Ceramics International* 47, 30178–30187.
774 <https://doi.org/10.1016/j.ceramint.2021.07.197>
- 775 Zinatloo-Ajabshir, S., Shafaati, E., Bahrami, A., 2022. Facile fabrication of efficient Pr₂Ce₂O₇
776 ceramic nanostructure for enhanced photocatalytic performances under solar light.
777 *Ceramics International* 48, 24695–24705.
778 <https://doi.org/10.1016/j.ceramint.2022.05.116>
- 779 Zuhua, Z., Xiao, Y., Huajun, Z., Yue, C., 2009. Role of water in the synthesis of calcined kaolin-
780 based geopolymer. *Applied Clay Science* 43, 218–223.
781 <https://doi.org/10.1016/j.clay.2008.09.003>
- 782

Highlights

- Activated metakaolin with $\text{H}_2\text{O}/\text{Na}_2\text{O}$ ratio higher than 20 and constant Si/Al and Na/Al atomic ratios
- Early stages of structuration evidenced by dynamic rheology and isothermal calorimetry
- Reaction degree of metakaolin deduced from quantitative analysis of NMR spectra
- $\text{H}_2\text{O}/\text{Na}_2\text{O}$ ratio influenced the reaction degree but not the structure of geopolymer
- Loss tangent deduced from rheometry and compressive strength can be correlated

Abstract

This study focused on the influence of high H_2O/Na_2O ratios (higher than 20) on the properties of metakaolin-based geopolymers in fresh and hardened states while keeping constant Si/Al and Na/Al atomic ratios. The increase in H_2O/Na_2O ratio from 21 to 34 resulted in a decrease of 7-day compressive strength from 10 to 0.025 MPa. This can be attributed to the influence of water on the reactivity of the precursor, which was demonstrated by nuclear magnetic resonance (NMR) spectroscopy and porosity evolution as the water is not chemically bound. Increasing H_2O/Na_2O ratio did not change the geopolymer structure of reaction products. A correlation was observed between the reaction degree deduced from NMR spectral decomposition and the cumulated released heat obtained using isothermal calorimetry. The maximum loss tangent, obtained using dynamic rheology, was linearly related to strength development.

CRedit authorship contribution statement

F. Souayfan: Investigation, methodology, formal analysis, software, writing - original draft;

E. Rozière: Supervision, formal analysis, writing - review & editing;

C. Justino: Funding acquisition, resources, supervision

M. Paris: Investigation, formal analysis, conceptualization;

D. Deneele: Investigation, formal analysis, resources;

A. Loukili: Funding acquisition, conceptualization, supervision.

Declaration of interests

The authors declare that they have no known competing financial interests or personal relationships that could have appeared to influence the work reported in this paper.

The authors declare the following financial interests/personal relationships which may be considered as potential competing interests: